ADVANCED HEALTHCARE MATERIALS
www.advhealthmat.de

Advances in Microfluidic-Based Core@Shell Nanoparticles Fabrication for Cancer Applications

Duarte R. S. Almeida, João Ferreira Gil, Antonio José Guillot, Jiachen Li, Ricardo J. B. Pinto,* Hélder A. Santos,* and Gil Gonçalves**

Current research in cancer therapy focuses on personalized therapies, through nanotechnology-based targeted drug delivery systems. Particularly, controlled drug release with nanoparticles (NPs) can be designed to safely transport various active agents, optimizing delivery to specific organs and tumors, minimizing side effects. The use of microfluidics (MFs) in this field has stood out against conventional methods by allowing precise control over parameters like size, structure, composition, and mechanical/biological properties of nanoscale carriers. This review compiles applications of microfluidics in the production of core-shell NPs (CSNPs) for cancer therapy, discussing the versatility inherent in various microchannel and/or micromixer setups and showcasing how these setups can be utilized individually or in combination, as well as how this technology allows the development of new advances in more efficient and controlled fabrication of core-shell nanoformulations. Recent biological studies have achieved an effective, safe, and controlled delivery of otherwise unreliable encapsulants such as small interfering RNA (siRNA), plasmid DNA (pDNA), and cisplatin as a result of precisely tuned fabrication of nanocarriers, showing that this technology is paving the way for innovative strategies in cancer therapy nanofabrication, characterized by continuous production and high reproducibility. Finally, this review analyzes the technical, biological, and technological limitations that currently prevent this technology from becoming the standard.

1. Nanotechnology in Cancer Therapy

Cancer is a complex, devastating disease with a global health impact. According to the World Health Organization cancer one of the top causes of death worldwide, it affects millions annually, causing numerous casualties.[1] Cancer treatment, encompassing surgeries, chemotherapy, radiation therapy, immunotherapy, and targeted therapies, incurs substantial costs that escalate due to prolonged care. Comprehensive addressing mandates ongoing research, improved prevention, early detection, and increased access to affordable, effective therapies.[2] A key challenge in cancer therapy is its effectiveness since some approaches do not adequately control tumor growth or prevent recurrence. For example, when approaches like radiation therapy are used as a standalone treatment, they can often harm surrounding healthy tissues, resulting in painful and highly uncomfortable experiences.[3] Ideally, cancer treatments should precisely

D. R. S. Almeida, J. F. Gil, G. Gonçalves
Centre for Mechanical Technology and Automation (TEMA)
Mechanical Engineering Department
University of Aveiro
Aveiro 3810-193, Portugal
E-mail: duarte99@ua.pt; ggoncalves@ua.pt
D. R. S. Almeida, J. F. Gil, G. Gonçalves
Intelligent Systems Associate Laboratory (LASI)
Guimarães 4800-058, Portugal

The ORCID identification number(s) for the author(s) of this article can be found under https://doi.org/10.1002/adhm.202400946

DOI: 10.1002/adhm.202400946

A. J. Guillot
Department of Pharmacy and Pharmaceutical Technology and Parasitology
University of Valencia
Ave. Vicent Andrés Estellés s/n, Burjassot, Valencia 46100, Spain
A. J. Guillot, J. Li, H. A. Santos
Department of Biomaterials and Biomedical Technology
University Medical Center Groningen (UMCG)
University of Groningen
Groningen 9713 AV, The Netherlands
E-mail: h.a.santos@umcg.nl
R. J. B. Pinto
CICECO—Aveiro Institute of Materials
Chemistry Department
University of Aveiro
Aveiro 3810-193, Portugal
E-mail: r.pinto@ua.pt
H. A. Santos
Drug Research Program, Division of Pharmaceutical Chemistry and Technology, Faculty of Pharmacy, University of Helsinki
Helsinki 00014, Finland

target cancer cells while sparing healthy cells to minimize side effects and preserve the overall well-being of patients. However, many existing therapies do not possess this level of selectivity, leading to adverse effects on healthy tissues and organs.[4]

To address these limitations, ongoing research is focused on developing more targeted and personalized cancer therapies. Precision medicine and immunotherapy are some of the promising approaches that aim to tailor treatments according to the idiosyncrasies of individual cancer patients.[5] Nanotechnology and targeted drug delivery mechanisms aim to improve the delivery of drugs specifically to tumor sites, minimizing damage to healthy tissues and enhancing the overall therapeutic outcome.[6] Nanomedicine presents a compelling field that revolves around the production and clinical application of precisely controlled NPs, commonly employed in therapeutic contexts as drug delivery systems or in diagnostics as highly effective contrast agents.[7] Additionally, the use of drug delivery-aided radiotherapy can amplify the effects of physical stimulation, thereby reducing the required dosage to induce cell death and facilitating precise targeting of the effects to the intended site.[3,8] Nowadays, NPs, also designated nanocapsules/carriers, have the ability to encapsulate and release selected therapeutic molecules in a precise and time-dependent manner.[9] They represent a not-yet conventional approach that has shown promising results over the last few decades, being able to solve significant challenges in the medical field, like inadequate drug solubility, low bioavailability, inherent drug instability, substantial adverse effects, and the absence of targeted drug delivery mechanisms.[10] In cancer therapy, these particles can traverse through the blood vessels and selectively target tumors.[5] More advanced drug delivery systems may even bind the surface to ligands that may actively target tumors.[11]

Specifically, CSNPs represent a unique combination of two materials, harnessing synergistic effects to integrate outstanding attributes from both components, which draws substantial scientific interest.[12] These particles are meticulously engineered to enable controlled drug release at specific sites, thereby minimizing the likelihood of potential side effects.[13] Operating as storage and carrier platforms across diverse applications, CSNPs release their core materials upon external stimulus activation, a process facilitated by shell rupture. This mechanism, crucial in drug delivery, employs biodegradable polymers for the shell, enabling triggered drug release in response to stimuli like temperature changes, electromagnetic fields, ultrasonic waves, and chemical signals. The adaptable polymers also afford control over surface and mechanical properties, ensuring gradual degradation. With its distinctive structure, the core-shell particle holds tremendous potential for triggered drug release, positioning it as an asset in drug delivery.[14]

A core-shell nanosystem's ability to encapsulate and stabilize active agents relies on two key attributes: one or multiple cores (commonly hydrophobic) and a hydrophilic exterior (commonly hydrophilic) (**Figure 1**). The inner region effectively encases the active agents, isolating them from the hydrophilic exterior and enhancing their aqueous stability by preventing hydrolysis. Simultaneously, the hydrophilic outer layer interacts with water, allowing the core-encapsulant complex to remain suspended in water.[15]

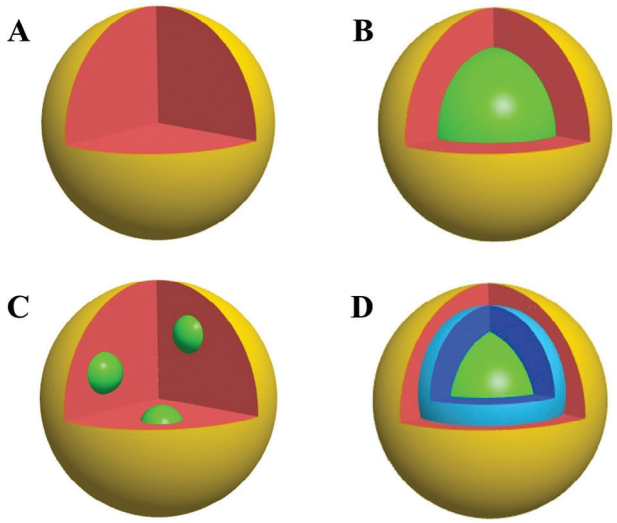

Figure 1. Different types of core-shell particles: A) Monophasic NP; B) core@shell; C) multicore@shell; D) core@shell@shell.

Studies have shown that maintaining a particle diameter of ≈100 nm or below yields the best results in enhancing blood-to-tumor transfer and prolonging their presence in tumor tissue.[9,16] This size range helps to minimize plasma protein adsorption and hepatic filtration, thereby improving effective tumor penetration.[17] The lower limit (10 nm) ensures avoidance of kidney clearance through excretion,[18] while the upper limit prevents removal from circulation by the spleen.[19,20] PEGylation has been used traditionally, with this specific aim of tuning the size, surface and solubility, as well as preventing the contact between the surface of the particle and other entities, which may induce degradation and clearance. This consists of the conjugation of polyethylene glycol (PEG) polymers to the surface of particles via functional groups.[21] However, it has also been observed that size-dependent distribution can be affected by the environment such as the tumor vasculature, since intercellular gaps are larger than normal, allowing larger NPs to exit the vessels.[22] Additionally, particle sizes above 200 nm activate the complement system, being quickly removed from the bloodstream.[18] As such, the ability to control NPs dimensions, along with the flexibility to tune both particle size and surface composition, are of paramount importance in regulating pharmacokinetics and biodistribution.[23,24] These capabilities enable the precise targeting of drug delivery for optimal therapeutic outcomes. Moreover, the capacity to engineer NPs characteristics, combined with the enhanced large-scale fabrication with high reproducibility achieved through microreactors compared to traditional methods, offers a potential platform for screening and identifying the finest properties of NP-based formulations tailored for specific therapeutic applications.[19]

Although CSNPs synthesized through batch processes find numerous applications, achieving homogeneity and optimizing reaction conditions often requires substantial effort. As a result, researchers are increasingly directing their focus towards synthesizing CSNPs using MF platforms, which offer more precise control and improved efficiency in the production process.[25]

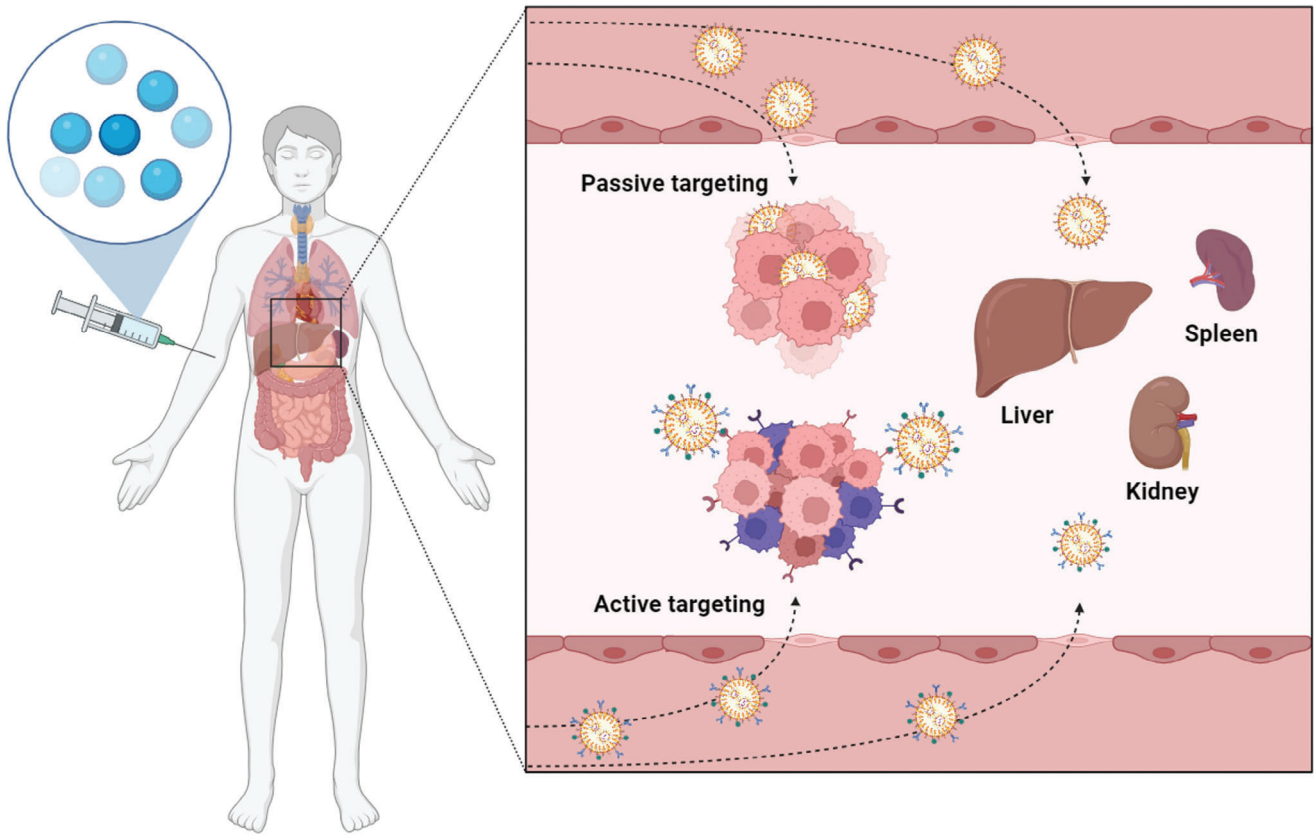

Figure 2. Scheme of the EPR effect. Sequestering and elimination of nanomaterials in circulation by the liver, spleen, and kidneys.

2. Clinically Available CSNPs in Cancer Diagnostic and Therapy

The field of nanomedicine is characterized by the precise delivery of active agents to specific cells through carefully selected nanomaterials. Cancer cells, due to their unique morphologies, surface chemistry, and surrounding environments, offer opportunities for effective diagnostics, therapies, or a combination of both, known as theranostics. Additionally, the codelivery of multiple active agents in a single formulation can disable drug resistance and therefore dramatically increase the efficacy of the drug.[26]

The delivery of drugs for precise targeting has been subdivided into active and passive targeting. Active targeting hinges on the principle of ligand-receptor interactions between the drug carrier and the cell.[11] using ligands like antibodies, aptamers, transferrin, and folic acid.[27] Conversely, passive targeting relies on the accumulation of delivered NPs onto cancer cells by extravasating through the discontinuous blood vessels around tumors. **Figure 2** shows the enhanced permeability and retention (EPR) effect, and it is commonly observed in solid tumors due to their characteristic abundance, leaky vasculature, and weak lymphatic drainage, attributed to dysfunctional lymphatic angiogenesis.[28]

However, it was reported that this effect is less pronounced in tissues like the pancreas, prostate, and liver, which host tumors with a comparatively lower degree of vascularity.[29] While this increased vasculature in some tumors facilitates the supply of oxygen and nutrients, it also allows the passage of molecules larger than 40 kDa (the limit for renal clearance), leading to their accumulation in the tumor microenvironment. Passive targeting relies on this principle to effectively target cancer cells.[30] Additionally, as time in circulation continues, NPs end up being sequestered by the liver and spleen, as well as eliminated by kidneys, which adds a certain level of strategy when considering new drug delivery systems.[31]

These NPs can be categorized based on their composition and structure, including polymeric, lipid-based, protein-based, and inorganic NPs, among others. Each type of formulation has its unique advantages and disadvantages, and the creation of composite hybrids can offer the opportunity to combine them, achieving the best of both worlds.

2.1. Lipid Nanoparticles (LNPs)

LNPs are characterized by a surfactant shell and a core that can exist in various forms, including liquid (micelles and liposomes), solid, or nanostructured (multicore).[32] These carriers are highly versatile, offering substantial drug loading capacity, the ability to encapsulate a wide range of substances, ease surface modification, enhanced biodegradability, controlled drug release, biocompatibility, and the lowest toxicity of all nanomedicinal formulations.[11,33] Consequently, LNPs are the most frequently employed carriers in the field of nanomedicine.[26]

At present, there are several markets and trial approved micellar CSNPs formulations for cancer therapy. Examples of these formulations include Paclical,[34] NK105 (paclitaxel, PTX),[35] NK911(doxorubicin, DOX),[36] NC-6004 (Cisplatin),[37] and NC-4016 (oxaliplatin and epirubicin).[38] Additionally, these NPs are also the primary vehicle for delivering siRNAs, which regulate the gene expression around the creation, growth, and metastasis of tumors.[39] In 2018, the first siRNA-based drug, Patisiran, was launched, built upon this principle.[40]

Liposomes are self-aggregated colloidal systems characterized by a bilayer structure composed of phospholipids, forming spherical vesicles with an aqueous core. Their formation occurs through self-assembly processes driven by the unfavorable interactions between phospholipids and water, typically in response to an increase in medium polarity. Liposomes generally are categorized based on size, including large unilamellar vesicles with sizes ranging from 100 to 1000 nm, small unilamellar vesicles ranging from 20 to 100 nm, and large unilamellar vesicles which are microstructures larger than 1000 nm, often referred to as giant liposomes.[41] Moreover, they can exhibit a multilamellar vesicle structure with multiple concentric layers.

These liposomal systems have gained extensive use in diverse applications in the biomedical and medical fields, particularly for nano-encapsulation of drugs and bioactive molecules. In recent decades, liposomes have been investigated as potential drug delivery systems, due to their amphiphilic nature, enabling the incorporation and conventional encapsulation of various drugs in the aqueous core or integrated into the hydrophobic shell.[42]

Following the approval of Doxil (1995), a PEGylated liposomal formulation of DOX, Myocet was developed as a possible alternative in 2000. Myocet is a non-PEGylated formulation of liposomal DOX approved for the treatment of metastatic breast cancer, often administered alongside cyclophosphamide. Notably, the absence of the PEG coating in this formulation prevents the occurrence of Foot-Hand Syndrome, a side effect associated with Doxil that results in swelling and pain in the hands and feet of the patients.[43] Additionally, other examples of liposomal formulations for cancer treatment include DaunoXome, Lipusu, and Kadcyla.[44] LNP research has seen an increasing interest over these last decades (particularly for cancer therapy). However, besides their use enabling the delivery of active agents with limited efficacy, their commercialization has also been mostly hampered by scalability issues.[45]

2.2. Polymeric Nanoparticles (PNPs)

Biodegradable polymers have also increasingly become the subject of extensive research, particularly for their potential applications in gene therapy, drug delivery, and imaging.[46] These polymers, which can be either natural or synthetic, can be organized in different configurations, including polymeric micelles,[47] dendrimers, cyclodextrins, or vesicles. The high diversity in polymeric properties makes PNPs extremely versatile. These capsules have enhanced physical and chemical stability, high encapsulation capacity, and tunable degradation rates, drug release, and cellular uptake, at the cost of an inherently lower degree of biocompatibility in some of the chosen materials.[29] The most commonly used materials in this context encompass poly(lactic-co-glycolic acid) (PLGA),[15,47–49] poly-ϵ-caprolactone (PCL),[15,50] poly(ethylene oxide) (PEO),[50] PEG,[47,51] polyethylene imine (PEI),[52] chitosan (CH),[53] among others.

In cancer nanotechnology, PLGA stands out as one of the most favored biodegradable synthetic polymers, due to its outstanding biocompatibility, biodegradability, mechanical, and adjustable degradation properties.[10] It has also shown relevance in cancer diagnosis. Focusing on using this polymer, Belletti et al. successfully improved the delivery of curcumin (CUR) using PLGA NPs conjugated with quantum dots.[54] This enhancement was achieved by enhancing cellular internalization and enabling easy tracking, thanks to the integrated imaging agent. Alternatively, chitosan and hyaluronic acid (HA) are examples of highly hydrophilic biopolymers that present high bioactivity and biocompatibility. In the specific case of HA, since many cancer cells overexpress the CD44 receptor, which predominantly binds to the repeating disaccharide units of b-D-glucuronic acid and N-acetyl-D-glucosamine that compose this polysaccharide, it emerges as an ideal candidate for cancer therapy.[55] A marketed example of PNPs being used in cancer therapy is Genexol-PM, a PTX-loaded PEG-PDLLA micelle.[56] This NP formulation gained clinical approval after showing controlled drug release, having been considered the best therapeutic candidate for chemoradiation therapy of its time.[57]

2.3. Protein-Based Nanoparticles

Protein-based NPs differ from PNPs in their biological properties, like superior biodegradability, temperature-dependent kinetics, and ease of modification. The protein class is so vast it allows for extra versatility and specificity.[58] These NPs combine the structural integrity of PNPs with the biocompatibility and bioactivity observed in biomolecule-based particles such as LNPs. The low immunogenicity of short peptides and compatibility of human proteins make them excellent choices for nanomaterials in drug delivery.[58] Several therapies based on this principle are already in clinical use, including Abraxane (an albumin-encapsulated PTX for pancreas cancer), Oncaspar (a PEGylated-L-asparaginase), and Opaxio (a poly-L-glutamic acid conjugate of PTX).[59]

2.4. Lipid-Polymer Hybrid Nanoparticles (LPNPs)

The mechanical advantage of polymeric materials can be combined with the biomimetic capacity of lipids to form LPNPs.[60] This integration offers various advantages, including surface functionality, high drug loading, the entrapment of multiple therapeutic agents, tunable drug release profiles, and good serum stability.[61] In addition to lower stability in relation to PNPs, one major disadvantage of using liposomes for drug delivery is their fast removal from blood circulation. This occurs because opsonins bind to the lipidic surface, leading to recognition by the reticuloendothelial system. This effect is particularly pronounced in the liver and spleen.[62] To minimize this effect, "stealth liposomes" have been developed, by functionalization with PEG.[4,63] Micelles and liposomes are commonly surface-modified with PEG, which allows for better-targeted delivery to precise

Table 1. NPs for cancer therapy and diagnostics approved by EMA and FDA that reach clinical trials or on the market.[26,65,69,70]

Name	NP	Active agent	Application	Company	Year
Doxil/Caelyx	PEGylated Liposome	DOX	Kaposi's sarcoma, ovarian, breast, multiple myeloma	Johnson & Johnson	1995
DaunoXome	Liposome	Daunorubicin	Kaposi's sarcoma	Galen	1996
LipoDox	PEGylated Liposome	DOX	Kaposi's sarcoma, ovarian and breast cancer	Taiwan Liposome	1998
DepoCyt	Liposome	Cytarabine	Neoplastic meningitis	Pacira	1999
Ontak	Recombinant protein	Deunileukin Diftitox	Cutaneous T-cell lymphoma	Les Laboratoires Servier	
Myocet	PEGylated Liposome	DOX	Breast cancer	Cephalon	2000
Eligard	Polymeric-protein	Leuprorelin acetate	Prostate cancer	Recordati Industria Chimica e Farmaceutica	2002
Abraxane	Albumin-encapsulated NP	PTX	Breast, pancreatic, and non-small-cell lung cancer	Abraxis/Celgene	2005
Oncaspar	Polymer-protein hybrid	L-asparaginase	Leukemia	Enzon-Sigma-Tau	2006
Lipusu	Liposome	PTX	Lung squamous cell carcinoma	Luye Pgarna	
Mepact	Liposome	Mifamurtide MTP-PE	Osteosarcoma	Takeda	2009
NanoTherm	Iron oxide NP	–	Glioblastoma	Magforce Nanotechnologies	2010
Marqibo	PEGylated Liposome	Vincristine	Acute lymphoid leukemia	Talon	2012
Kadcyla	Monoclonal antibody	DM1	Breast cancer	Roche Genentech	2013
Onivyde	PEGylated Liposome	IRI	Pancreatic cancer	Merrimack Pharma	2015
DHP107	LNP	PTX	Gastric cancer	Daehwa Pharmaceutical	2016
PROMITIL	PEGylated Liposome	Mitomycin-C	Solid tumors	Lipomedix Pharmaceuticals	
Oncoprex	Liposome	FUS1 (TUSC2	Lung cancer	Genprex	
Halaven	Liposome	Eribulin mesylate	Solid tumors	Eisai	
Vyxeos	Liposome	Cytarabine/Daunorubicin	Acute myeloid leukemia	Celator/Jazz Pharma	2017
Apealea	Micelle	PTX	Ovarian, peritoneal, and fallopian tube cancer	Oasmia Pharmaceutical AB	2018
Pazenir	Albumin-encapsulated NP	PTX	Breast, pancreas, and lung cancer	Ratiopharm GmbH	2019
Hensify	Hafnium oxide NP	–	Locally-advancer soft tissue sarcoma	Nanobiotix	

DM1: Emtansine; DOX: doxorubicin; IRI: irinotecan; LNP: Lipid NP; LPNP: Lipid-polymer NP; PTX: paclitaxel.

tissues, transport, and retention,[32] as is the case in lymph node targeting.[40]

Doxil (or Caelyx in Europe) was the first PEGylated nanoliposome drug approved in 1995 by the U.S. Food and Drug Administration (FDA),[64] used to treat ovarian cancer and AIDS-related Kaposi's sarcoma by delivery of DOX. After this approval, several other PEGylated liposomal formulations have been developed and marketed: LipoDox, Myocet (formulations of DOX), Marqibo and Onivyde (vincristine and irinotecan, respectively), and PROMITIL (mitomycin-C) are some examples.[63,65,66]

CSNPs have gained a strong relevance for fighting cancer, as can be clearly proven by the large number of nanomedicines in clinical uses, as summarized in **Table 1**. Therapy, diagnosis, and theranostics for several types of cancer have been approached with these NPs, using different combinations of encapsulants and cancer-active compounds. DOX and PTX are the most common chemotherapeutical agents in cancer therapy, having become staples of the field. Their combined use has been tested before, and, although effective, it has proven quite cardiotoxic.[67] Additionally, immunological issues arise from having these molecules circulating freely.[68] Challenges like these create the need for nanocarriers capable of delivering directly to the targeted cells to avoid the action of the active agents against healthy tissues, promoting significative secondary effects in patients.

3. Microfluidic Fabrication of CSNPs

3.1. MF-Assisted Nanoprecipitation and Emulsification Processes

MF-assisted fabrication of particles entails an inherent mixing process of two or more solvents,[71] which has a crucial impact on the final properties and features of the produced nano-sized systems in terms of homogeneity and size.[72] This technology's main advantages in comparison with bulk methods are rigorously linked to this mixing process. On one side, MFs allow a fast mixing of fluids in the microchannels or capillaries, and on the other side, the reduced scale of these structures (submillimeter range) in the MF devices increases the surface-to-volume ratio and, consequently, the effects of surface tension and viscous forces.[73] Therefore, the properties of the solvents used

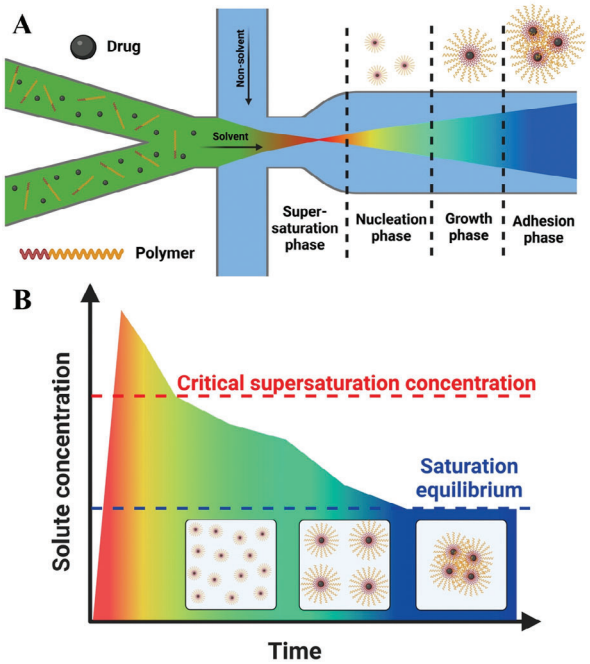

Figure 3. A) Schematic of a MF-assisted synthesis of micelles via nanoprecipitation; B) Different phases of the supersaturation-precipitation dynamic.

have an enormous impact on the chosen MF strategy. In broad terms, nanoprecipitation occurs under a continuous flow system when a pair of solvents are miscible,[74] whereas emulsification takes place in a segregated flow system when the solvents are immiscible.[75]

In the first case, as a "bottom-up" approach where an assembly of molecules generates supra-molecular entities,[61] a solvent fluid containing the precursors diffuses through the non-solvent fluid, creating a highly supersaturated environment for them and leading to their precipitation.[76] This process involves four phases: supersaturation, nucleation, growing, and adhesion (represented in **Figure 3**A).[77]

The supersaturation phase occurs when the solute amount is higher than the value given by the equilibrium saturation value. The supersaturation ratio (Sr) can be mathematically calculated by Equation 1:[78]

$$Sr = \frac{Cs}{C\infty} \tag{1}$$

where Cs corresponds to the ratio of the particle solubility at the interface, and $C\infty$ represents bulk solubility. To increase the thermodynamic stability, the nucleation starts when the supersaturation reaches a critical level that is specific to the solvent/non-solvent pair, and the energy barrier is overcome (as Equation 2 and the graph in Figure 3B show):[78]

$$\Delta G = \frac{16\,\pi\,\sigma^3\,mv^3}{3\,K^3\,T^2\,(ln\,Sr)^2} \tag{2}$$

where, σ corresponds to the interfacial tension; mv refers to the molar volume of the solute; K is the Boltzmann constant; and T is the temperature. The nucleation step involves a size increase of the nuclei, caused by the addition of solute molecules. This happens until these nuclei reach a stable size, after which the solution supersaturation is depleted. The growing phase still decreases the solute concentration, where the addition and adsorption of single molecules to the particle surface occur. Once the concentration of free-solute is lower than the equilibrium saturation value again, the condensation-boosted growth ends, and the particles adhere together by attractive forces – mainly Van der Waals or hydrophobic interactions (Figure 3B).[79] The coagulation of the formed particles is highly related to their collision frequency. Therefore, it depends on the concentration and size of the particles and can be prevented using stabilizing agents.[80]

In contrast, emulsions refer to the dispersion of stabilized liquids within a continuous, immiscible liquid. This phenomenon has found widespread application across various industries. Emulsions can take the form of two-phase dispersions: oil-in-water (O/W) or water-in-oil (W/O) emulsions, known as simple emulsions. Additionally, they can exist as more intricate multiphase dispersions called multiple emulsions, comprising larger drops containing single or multiple inner compartments. Multiple emulsions, such as oil-in-water-in-oil (O/W/O) and water-in-oil-in-water (W/O/W), serve as crucial formulations in the synthesis of micro- and nanocapsules, which are utilized to protect active substances from chemical degradation or evaporation and enable delayed or triggered release mechanisms. These capsules find applications in diverse areas, providing controlled and sustained delivery of substances for various purposes.[81] MF methods offer a reliable alternative to classical emulsification techniques. Unlike bulk production, which involves emulsion solvent evaporation, MF methods generate micro/nanospheres drop-by-drop, yielding a much higher level of monodispersity.[14,61] In the nanoprecipitation approach, MFs is a technique that makes use of miniature devices to process or manipulate small volumes of liquids within microchannels (typically in the micro- or nanoliter range). As such, this technology allows for greater control over mixing, heat, and mass transport in comparison to conventional bulk methods. Furthermore, even though bulk emulsification enables the incorporation of different functional compounds separately into both inner and outer drops, MFs can achieve an extraordinary level of control in the introduction of distinct contents into the inner droplets in a highly regulated manner within the middle phase of multiple emulsions.[81] This is one of the main reasons behind the rapid advancements in the field of nano-micro lipid systems, which is evident from the substantial rise in publications in the domains of pharmacology and pharmacy.[61]

3.2. Flow Regimes and Patterns in MF-Assisted Fabrication of NPs

MF flow patterns refer directly to the behavior of the fluid in microscale structures.[82] The main flow patterns in a MF device are laminar and turbulent, which can be predicted by the Reynolds number (Re), determined according to Equation 3:[83]

$$Re = \frac{\rho\,v\,L}{\mu} \tag{3}$$

where, ρ stands for the density of the fluid; v corresponds to the fluid velocity; L stands for the linear dimension; and μ

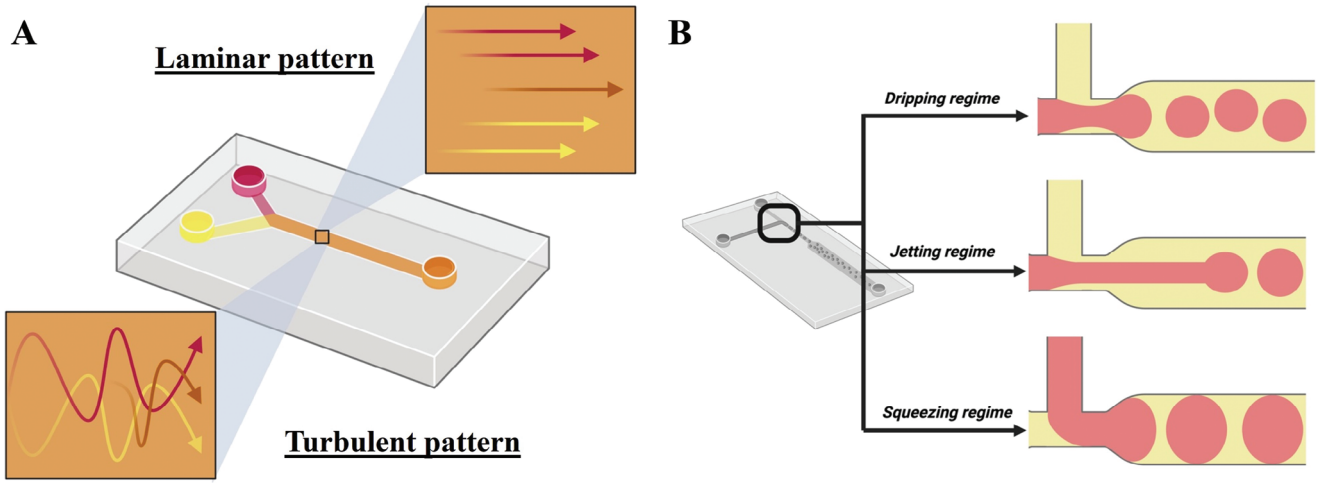

Figure 4. A) Laminar versus turbulent flow; B) Dripping, jetting, and squeezing regimes.

corresponds to the dynamic viscosity of the fluid. On one side, high *Re* values are associated with turbulent flows and can be achieved by increasing the flow rate of a fluid, its density, or by decreasing the viscosity. By contrast, low *Re* values describe laminar patterns. are no clear cut-off values for considering *Re* as high or low; generally, a $Re < 2000$ is deemed low for a laminar pattern, whereas $Re > 5000$ is typical in turbulent regimes. The transition phase, $2000 < Re < 5000$, shows a hybrid behavior with features of both patterns. The turbulent pattern implies the chaotic motion of the fluids, which move in all space dimensions, while the laminar pattern is defined by parallel streamlines flowing linearly with little mixing based mainly on diffusion (**Figure 4A**).[84] In the latter scenario, the random motion of molecules within the surrounding environment (diffusion) and the transport from the bulk motion of the fluid (convection) have a special importance. Both motions are reflected by the Péclet number (*Pe*), as Equation 4 shows:[85]

$$Pe = \frac{U\,H}{D} \tag{4}$$

where, *U* stands for the average speed of the flow; *H* corresponds to the length of the system perpendicular to the flow direction; and *D* stands for the mass diffusion coefficient of the molecule or particle of interest. Thus, when $Pe < 1$, diffusive transport is more efficient – as opposed to convection – and commonly achieved under laminar flow (and with the use of small volumes).[86] Moreover, a reduced transfer of drugs from the dispersed phase contributes to a higher drug encapsulation efficiency in the formulations produced by MF.[87]

In droplet MFs, two immiscible fluids are mixed and the surface instabilities between those phases determine the droplet type and regime. Droplet formation is a complex process affected by numerous factors, such as fluid viscosity, density, surface tension, flow speed, etc., that determine how droplets are broken off from the dispersed phase.[88] Three regimes (dripping, jetting, and squeezing) have been widely studied to understand the physical mechanisms involved and predict the size, diameter and frequency of droplet production (Figure 4B).[89]

In the dripping regime, the drops break off from the inner injection source and are dragged downstream by the continuous outer flow. In the jetting regime, the dispersed fluid flows through the continuous phase, and the droplets are pinched off only when the jet destabilizes far from the injection source.[90] Finally, the squeezing regime is characterized by droplet formation as plugs with a length larger than the microchannel width.[91] The balance between the surface tension and viscous forces can determine how and when droplets or jets are formed. The relation of the forces can be described by the Weber (*We*), Bond (*Bo*) and capillary (*Ca*) numbers, as determined in Equations 5–7:[92]

$$We = \frac{\text{inertial force}}{\text{interfacial tension force}} = \frac{\rho\,Q\,U}{2\,\pi\,r\,\sigma} \tag{5}$$

$$Bo = \frac{\text{buoyancy force}}{\text{interfacial tension force}} = \frac{\Delta\rho\,g\,r^2}{\sigma} \tag{6}$$

$$Ca = \frac{\text{viscous shear force}}{\text{interfacial tension force}} = \frac{\mu\,v}{\sigma} \tag{7}$$

where, ρ corresponds to the density of the dispersed phase; *Q* stands for the flow rate of the dispersed phase; *U* aims for the velocity of the dispersed phase; *r* corresponds to the wetting radius of the dispersed phase at the tip of the inlet source; $\Delta\rho$ refers to the density difference between dispersed and continuous phases; μ corresponds to the dynamic viscosity of the most viscous fluid in the system; v corresponds to the fluid velocity; and σ stands for the interfacial tension. It has been experimentally observed that dripping occurs when $We + Bo < 1$, and the interfacial tension dominates the behavior of the fluid. Meanwhile, jetting cases occur when $We + Bo > 1$.[93] In addition, the dripping regime is associated with a weak flow of both liquids,[90] whereas the jetting regime needs higher flow rates (which requires a continuous phase flow higher than the dispersed phase flow).[91] Regarding the *Ca*, as a measure related to the surface tension force and the drag force, it has been observed that it is inversely proportional to the drop diameter.[94] Thus, the drop size does not depend upon the fluid of the dispersed or inner phase, and it is only related to the velocity of the outer fluid or continuous phase. In

this sense, the variation of the flow rate ratio (FRR) between the inner and outer fluids does not affect the droplet size. However, it does affect the droplet generation frequency, since, for the same droplet size, a different inlet and outer drag force are generating the drops.[95]

3.3. MF Devices

Typically, MF devices come in sizes that span from a few millimeters down to micrometers. They are primarily defined by featuring at least one channel with dimensions smaller than 1 mm.[61] These devices can be tailored to desired shapes and dimensions and fabricated with several materials, most commonly using polydimethylsiloxane (PDMS) polymer,[49,50,52,47,96–99] as well as glass.[19,32,100,101] PDMS stands out as the predominant material for MF device fabrication due to its numerous advantages, including ease of fabrication, optical transparency, gas permeability, and cost-effectiveness. This versatility has established PDMS as a key material for applications in bioassays and targeted drug delivery systems through implantable MF devices.[102] However, PDMS MF devices preparation usually requires usually the use of clean rooms, increasing their production cost in terms of needed infrastructure.[103,104] These also present other drawbacks; for example, the non-specific adsorption and permeation of hydrophobic molecules, poor solvent compatibility, channel fouling due to 2D flow geometries, and deformation under high-pressure conditions.[10,96] In addition, these are susceptible to degradation, due to their sensitivity to certain organic solvents, acids or bases. This limits the compatibility of these chips with different synthesis methods where such solvents are required.[105] Moreover, the hydrophobic nature of PDMS is an extra challenge when working with common polymers, like PLGA, that aggregate on the walls because of their hydrophobicity, resulting in clogging of the channels.[106] Although the surface of channels can be modified by chemical or physical methods,[107,108] the process is often time-consuming and expensive. Glass capillaries-based devices are the main alternative, as they can be homemade by using specific equipment, without the need of specialized laboratories. As a material for preparing glass capillaries, borosilicate shows interesting properties such as chemical resistance, mechanical and thermal stability, and superior optical transparency.[109] However, the design of different configurations is limited, and the manual production is tedious and requires optimal manual skills.[110]

Numerous manufacturing techniques are available for producing microdevices. Noteworthy among them are photo and soft lithography,[19,49,52,97,98,99] micro-milling,[111] etching,[19,32] and micromachining and laser ablation.[61] Soft lithography is the primary method employed to create microstructures in PDMS. In constructing glass capillary MF devices, a standard procedure consists of pulling capillaries through a fine tip to achieve precise orifice sizes. These capillaries are then co-axially assembled inside a wider square or circular capillary. Finally, they are glued onto a glass slide to complete the device construction.[13,32,101]

The fabrication of CSNPs can be achieved either by continuous phase or segregated phase flow MFs. Droplet-based MFs (segregated phase flow) yield remarkably consistent and uniform particles with high reproducibility and monodispersity.[112] However, the literature describes that the use of droplet-based MFs primarily leads to the production of microscale particles. In contrast, particle synthesis in continuous MFs tends to result in nanoscale particles.[48,61] It is worth noting the apparent resurfacing of droplet-based MFs in the form of open systems, which have shown a significant advantage regarding ease of use and accessibility, by setting aside complex designs and fabrication methods at the cost of liquid evaporation issues and a lower throughput (due to not using syringe pumps but rather human operation).[113]

By contrast, continuous phase flow is usually the preferred strategy for engineering CSNPs since it creates a homogeneous environment that is favorable to NPs formation with a narrower size distribution.[114] Another advantage of continuous phase flow MFs is the uniform concentration, heat, and fluid profile within the inner fluid, which prevents particle generation close to the channel wall, effectively reducing the risk of channel clogging.[48]

The flexibility of MF chips comes from the vast selection of micromixers, channel designs, and structures available. When it comes to achieving optimal mixing for NP formulations using passive micromixers, various systems are employed. Simple channel junctions (crossflow mixing) may need to be followed by micromixing channels with streamline disturbances like zigzag, chicanes, or serpentines to enhance further mixing phenomena.[32] Other more complex setups can operate independently, like hydrodynamic flow focusing (HFF), confined impinging jet mixers (CIJM), or multi-inlet vortex mixing (MIVM).

The architecture of MF chips and the injection order of solvents have a notable impact on the final features of the produced particles, such as the mechanical properties. For example, Sun et al. developed a two-step continuous phase flow MFs device to produce two prototypes of PLGA-lipid coated NPs with different rigidity properties (**Figure 5**A–C).[115] This device consisted of a HFF system followed by a spiral mixing channel. First, the PLGA core could be successfully produced by nanoprecipitation, being then coated in the second stage because of the hydrophobic attraction between the lipid tail and PLGA. However, when the injection order was changed by introducing the lipid solution at the first step and the polymer solution at the second one, lipids formed a liposome-like vesicle followed by reassembly onto the surface of PLGA core at the second stage after an effective mixing. This strategy allowed the production of particles with the same size, but with different amounts of interfacial water between the polymeric core and the lipidic shell. This led to distinct cellular uptake properties since the more rigid lipidic envelope facilitated movement through the membranes. Increasing the number of stages in the system makes it possible to create a double PLGA-lipid shell NP to encapsulate water-soluble agents like siRNAs, as Zhang et al. demonstrated (Figure 5D–F).[116] The co-precipitation of PLGA and cationic lipids in water with an extra stage allowed the fabrication of a reverse micelle and then a PLGA shell.

Similarly, the final step in a spiral channel step provided the outer envelope with anionic lipids. In addition to the architecture design and injection order, the 3D geometry of the devices has also shown to dramatically affect the resultant particles. The size of polymeric PLGA NPs can be successfully decreased when MF chips have a 3D arch or double spiral geometry when compared

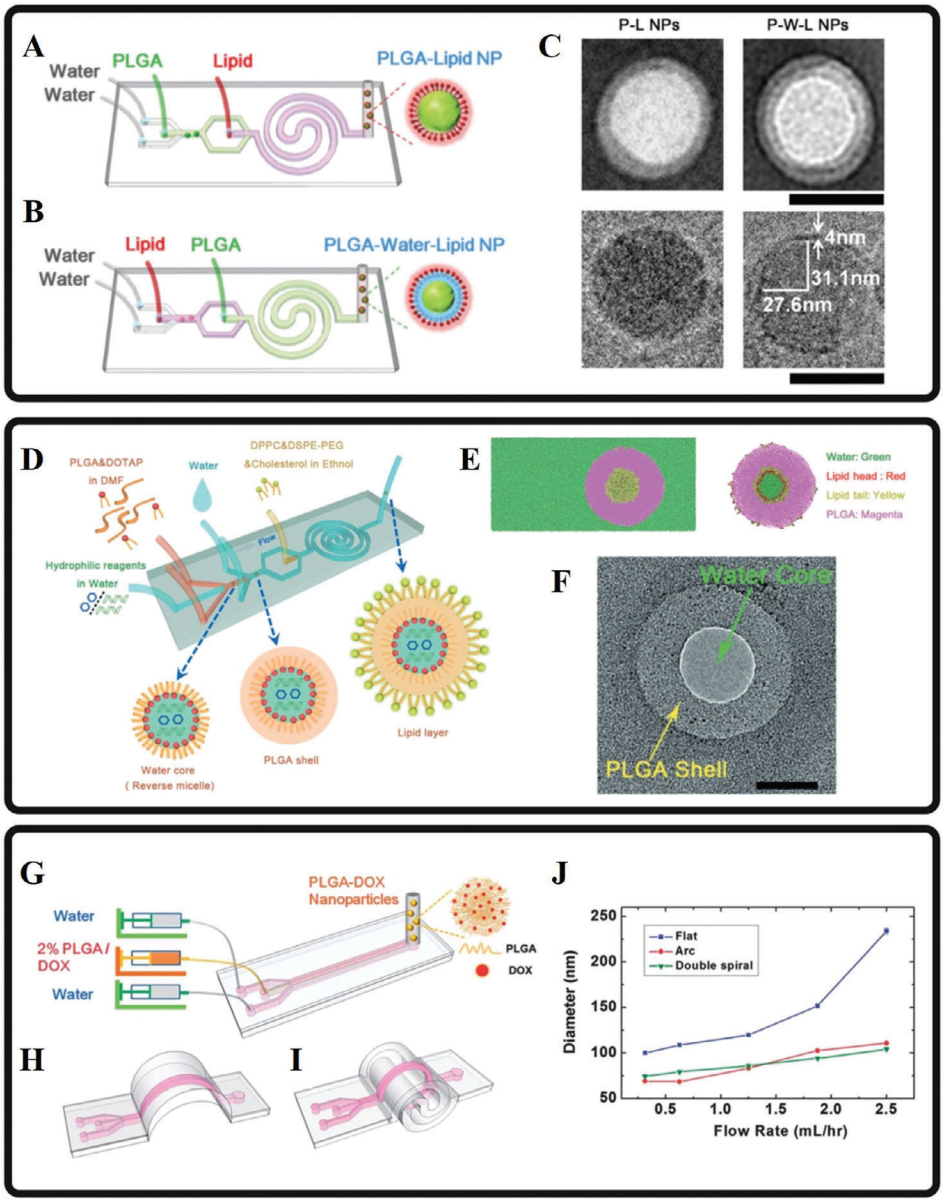

Figure 5. A) Illustration of a flat-2D MF chip to synthesize PLGA-lipid coated NPs; B) Illustration of a flat-2D MF chip for synthesizing PLGA-water-lipid coated NPs; C) TEM and Cryo-TEM images of PLGA-lipid coated NPs and PLGA-water-lipid coated NPs (scale bar 50 nm); adapted with permission.[115] Copyright 2024, John Wiley and Sons; D) Three-stage MF chip for the synthesis of water core/PLGA shell/lipid layer rigid nanovesicle; E) Snap shots of dissipative particle dynamics simulation of particle formation. Water is shown in green, lipid head in red, lipid tail in yellow, and PLGA in magenta; F) TEM image of a double PLGA-lipid shell NPs (scale bar 50 nm); adapted with permission.[116] Copyright 2024, John Wiley and Sons; G) Illustration of a flat-2D MF chip for synthesizing Docetaxel-loaded PLGA NPs; H) Illustration of an arch-3D MF chip for synthesizing Docetaxel-loaded PLGA NPs; I) Illustration of a double spiral-3D MF chip for synthesizing Docetaxel-loaded PLGA NPs; J) Impact of 2D and 3D MF devices architecture on the size of PLGA particles. Adapted with permission.[117] Copyright 2009, RSC Pub.

to two-dimensional flat architecture. This is a consequence of the decrease in mixing time derived from a shorter mixing distance (Figure 5G–J).[117]

3.4. HFF

HFF harnesses the laminar regime, usually characterized by a low *Re*.[61] In a continuous phase flow system a slender stream of fluid comprising NPs precursors dissolves and flows parallel with an antisolvent (e.g., water or buffer solution) from side channels. As mentioned above, due to the laminar flow regime within the device, rapid mixing occurs primarily through diffusion.[7,10] HFF can be effectively employed in both 2D and 3D configurations, using three inlet streams with a cross-shaped geometry (**Figure 6**).

Although this method is commonly used to produce LNPs, limited flow rates hinder scalability and high throughput,

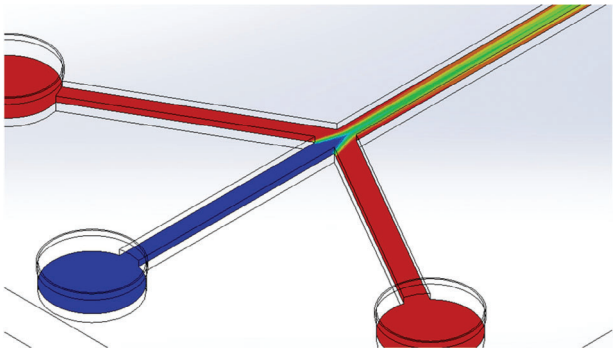

Figure 6. Schematic of a HFF setup.

making it less suitable compared to more efficient techniques that have since emerged.[61]

As estimated by Karnik et al., the correlation between mixing time and various parameters is described by Equation 8:[47]

$$t_{mix} = \frac{w_f^2}{4D} \sim \frac{w^2}{9D}\left(\frac{1}{\left(1+\frac{1}{R}\right)^2}\right) \quad (8)$$

where, D is the diffusivity of the solvent, W_f is the width of the focused stream, W is the channel width, and R is the FRR of the middle stream to the flow rate of the sheath stream. As such, W_f relies on both the channel's width and the FRR; smaller channels with higher flow rates result in shorter mixing times, which leads to smaller particle sizes and improved uniformity.[19,101] To reduce the size of NPs, one can also increase the total flow rate of the streams while maintaining their ratio constant so the streams meet each other at higher velocities, decreasing the mixing time scale. Because of this, as explained by Liu et al., the NPs formed are smaller and more finely controlled.[10] In MF nanoprecipitation, this is achieved by inducing a rapid solvent shift, transitioning from an organic to a non-solvent, creating a highly supersaturated environment for all substances involved. Consequently, nucleation and diffusion-limited aggregation of precipitates take place.[19] Because of this, HFF provides superior control over NP synthesis when compared to more traditional methods. Furthermore, designing HFF setups with varying channel widths and adjusting the FRR, makes it possible to produce highly customizable NPs with precise size and size distribution. Achieving a smaller particle size often requires reducing the dimensions of the device, which can lead to low throughput. Consequently, considerable time to produce an adequate number of NPs. Additionally, a high FRR results in a highly diluted NPs solution at the device outlet.[10] However, it has also been extensively described that the size of liposomes can be decreased by increasing the FRR between the aqueous phase and organic phase in a HFF approach (**Figure** 7A,B), avoiding the disadvantages of increasing the total flow rate or reducing the dimensions of the MF devices.[118,119] Exercising precise control over the NP size eliminates the need for post-synthesis purification steps, typically required to remove macroscopic aggregates formed during bulk synthesis. This fact leads to a reduced loss of material and significantly enhances productivity.[19] Moreover, HFF permits the fabrication of NPs with adjustable surface properties, achieved by using functionalized lipid or polymer precursors. These functionalized precursors enable the creation of NPs with specific surface modifications, such as PEGylation, single targeting ligands, or dual ligands, further expanding the versatility and applicability of HFF in NP synthesis.[10] The HFF method was proven to be a high versatile solution for the controlled synthesis of the CSNPs. **Table** 2 showcases a few examples of CSNPs produced using the HFF method.

Structurally like the HFF setup are the crossflow mixers. Specifically, the T-, Y-, and X-shaped junctions are among the most common MF setups used in synthesizing NPs due to their ease of fabrication and operation. These junctions pump the dispersed phase against the continuous phase at a certain angle (**Figure** 8), subjecting the fluids to shear forces that result in droplet formation.[123] The use of these cross-flow devices offers noteworthy alternatives, such as easy control of the flow regime by controlling the capillary number and FRR. For instance, Loizou et al. reported that dripping regime is observed at lower flow rate ratios between dispersed and continuous phases and squeezing at higher ones when the capillary number remains constant (**Figure** 9A). In addition, the droplet size tends to vary proportionally to the FRR between the dispersed and continuous phases.[124] Sheng et al. also reported the impact of the relation between capillary number and the phase flow ratio on the flow regime (Figure 9B).[125]

Although these junctions present some mixing limitations, their straightforward production can be advantageous.[32] To overcome those limitations, these geometries are often paired with chaotic advection-based micromixing systems, such as the staggered herringbone micromixer (SMH),[126] or baffle mixers (BM).[127] An interesting example was studied by Lallana et al. that compared the mixing efficiency between a micromixer-aided Y-junction setup and a X-junction crossflow mixer in the synthesis of poly (D, L-lactic acid-co-caprolactone) NPs for the delivery of PTX.[128] The results indicated that the micromixer allowed the formation of smaller particles. **Table** 3 summarizes the different combinations of junctions, crossflow setups, and operation conditions reported so far in the literature for synthesizing CSNPs.

To overcome issues inherent to PDMS-based devices, borosilicate glass capillary devices have emerged as a promising solution for HFF applications towards a 3D axisymmetric flow focusing approach (**Figure** 10A).[130] They offer several advantages over PDMS, including inertness to most solvents and minimal deformation due to its high Young's modulus, ensuring consistent operating conditions.[10] In this architecture, both phases flow in opposite directions of the outer channel, meeting at the entrance of the inner capillary, where droplets are formed.[131] The physical principles behind this configuration are complex; however, it allows different regimes such as dripping and jetting.[132] Bertoni et al. produced multicore@shell particles responsive to reactive oxygen species (ROS) and pH (Figure 10B).[133] Particularly, ROS-responsive cores were made of a phenylboronic-modified dextran by bulk nanoprecipitation (BN) in which Rifaximin was loaded. Then, by a 3D axisymmetric flow focusing emulsification, those cores were incorporated in pH-responsive methylcellulose acetate succinate particles.

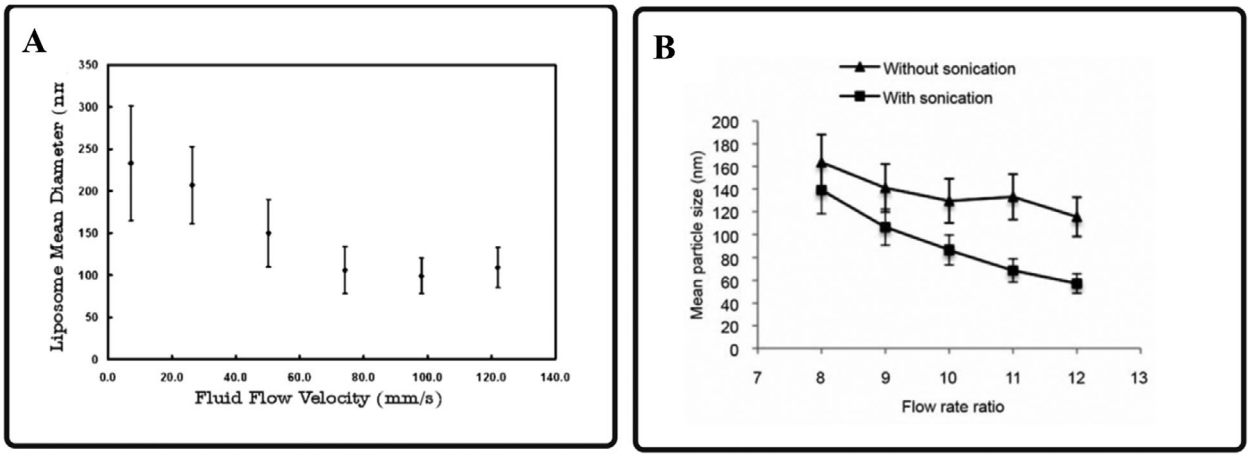

Figure 7. A) Evolution of particle size of liposomes when increasing the FRR between the aqueous phase and organic phase in Jahn et al. study;[119] reproduced under public domain; B) Evolution of particle size of liposomes depending on the FRR. Reprinted with permission from.[118] Copyright 2024, International Institute of Anticancer Research (IIAR).

Table 2. Examples of CSNP produced by HFF methods for drug delivery in cancer therapy.

Core@Shell	NP size [nm]	Active agent	Channel size [μm]	Channel length [mm]	Center flow rate [μL $mi^{-1}n$]	Side flow rate [μL $mi^{-1}n$]	Ref.
QD@PLGA-Lipid	<100	QD	50 × 60	–	50	5	[96]
β-carotene@PluronicF127	70	*β*-carotene	50 × 130	30	17	–	[19]
SMVT@Lipoproteins	8 – 31	Simvastatin	400 × 2 000	–	5000	1000	[97]
PLGA@PEG polymeric micelle	10 – 50	Dtxl	60 × 20	10	0.3 – 1	10	[47]
PEGylated monomolecular LNP	38	siRNA	74 × 100 – 200	1640	1.7	15	[120]
PCL@PEO	15 – 69	PTX	150 × 100	18	100, 200, 400		[50]
PEGylated liposome	100	–	20 × 60	10	28.8		[20]
PTX/CUR@TA/Fe III complex	100 – 200	PTX/CUR	760	–	67 – 3600		[98]
PLGA/PP@HA	100 – 123	IRI	125 × 350	–	100	–	[121]
PEI-b-PCL@Lipids	120	siRNA	60 × 300	5	3.3	33 – 250	[52]
Magnetic core@CH	104	Cisplatin	100-150	0.2	1.7 – 17	33	[99]
CH@SPC:Chol	77 – 113	Gd-DTPA and IRI	160 × 150	–	3	41	[122]

CH: Chitosan; Chol: Cholesterol; CUR: curcumin; Dtxl: Docetaxel; HA: hyaluronic acid; IRI: irinotecan; NP: NP; PCL: polycaprolactone; PEG: polyethylene glycol; PEI: Polyethylimine; PEO: polyethylene oxide; PLGA: poly-lactic-co-glycolic acid; PP: PF68 and PF127 (amphiphilic poloxamers); PTX: paclitaxel; QD: quantum dot; SMVT: Simvastatin; TA: Tannic acid.

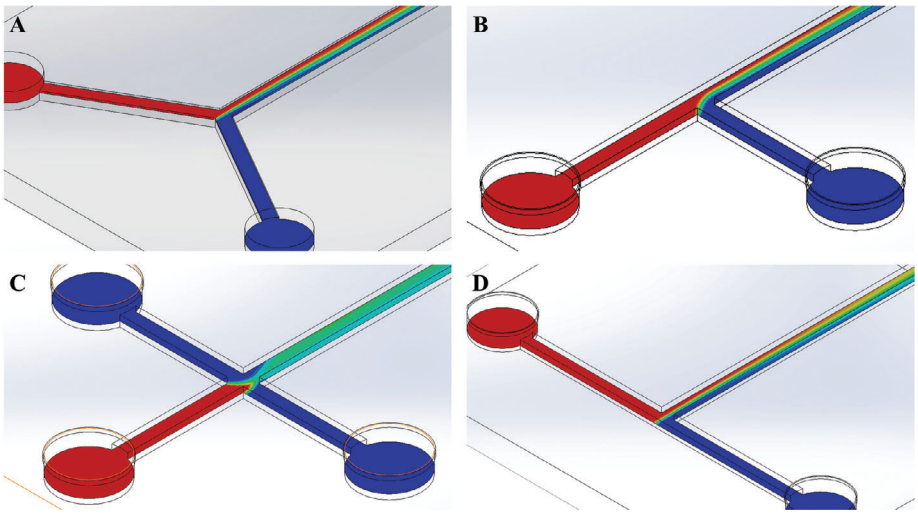

Figure 8. Scheme of crossflow MF junctions: A) Y-junction; B) T-junction with 90° angle; C) X-junction; D) T-junction with 180° angle).

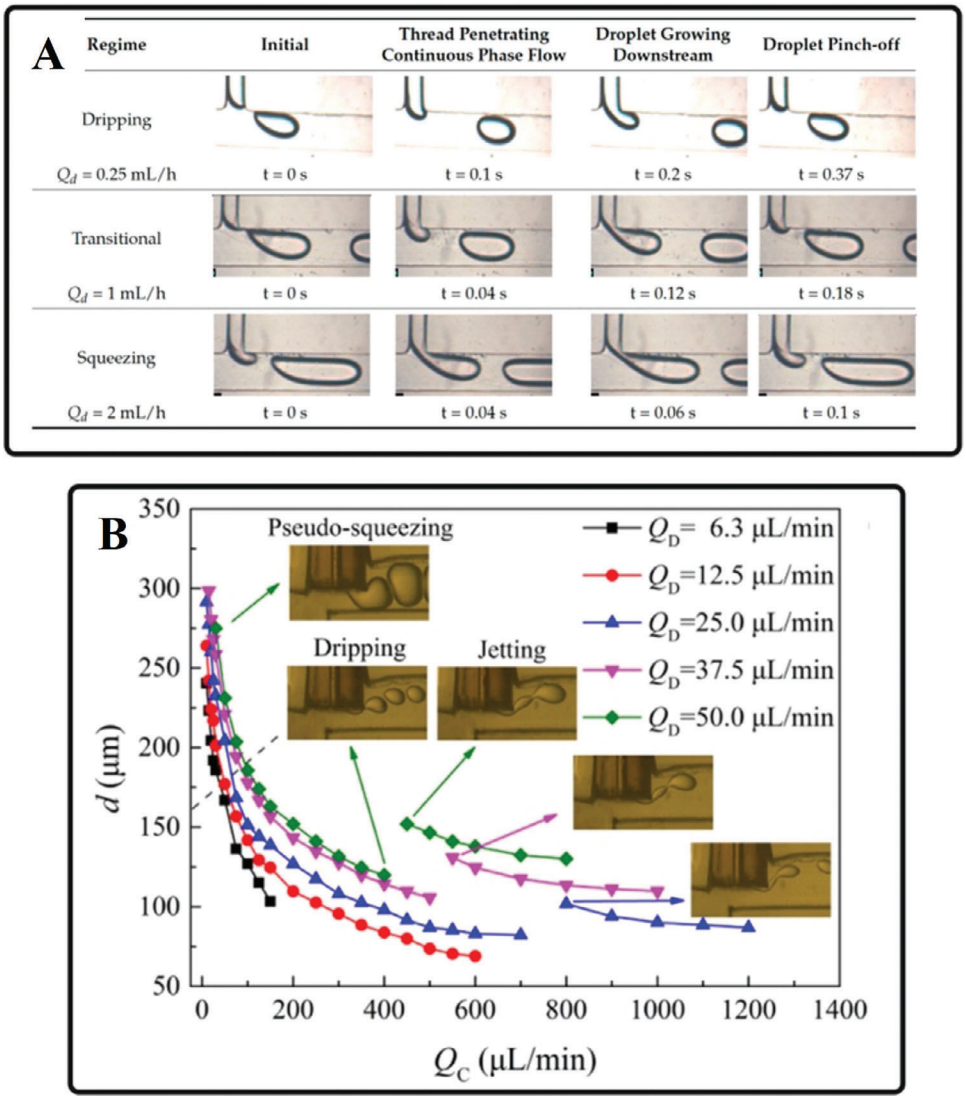

Figure 9. A) Droplet generation in dripping, squeezing and transitional regime at a constant capillary number (Ca = 0.0566) and continuous phase flow rate, when dispersed flow rate varies; reproduced under the terms of the CC BY 4.0 license.[124] Copyright 2013, MDPI; B) Variation of the droplet size and flow regime depending on the continuous and dispersed flow rates. Reproduced with permission.[125] Copyright 2024, Elsevier B.V.

Table 3. Crossflow MFs in CSNP synthesis for drug delivery in cancer therapy.

Junction	Core@Shell	NP size/nm	Active agent	Micromixer	Channel size [μm]	Channel length [mm]	Flow rate [μL $mi^{-1}n$]	Secondary flow rate [μL $mi^{-1}n$]	Ref.
X	PEGylated PLCL	80 – 160	PTX	Baffle mixer	–	–	2000	–	[128]
Y		30 – 120	–	SRM	–	–		–	
	Liposome	20 – 100	siRNA	Baffle mixer	100 × 200	3	500	–	[129]
	Labrafac oil@Surfactants	25 – 100	–	Baffle mixer	300 × 1500	500	2000 – 10000	100 – 500	[32]
	PEGylated multi-core liposome	200 – 800	pDNA	SHM	–	–	2000 – 8000	–	[126]

pDNA: Plasmid DNA; PEG: polyethylene glycol; PLCL: poly (D,L-lactic acid-co-caprolactone); PTX: Paclitaxel; SHM: Staggered Herringbone Micromixer; siRNA: small interfering RNA; SRM: split and recombine mixer.

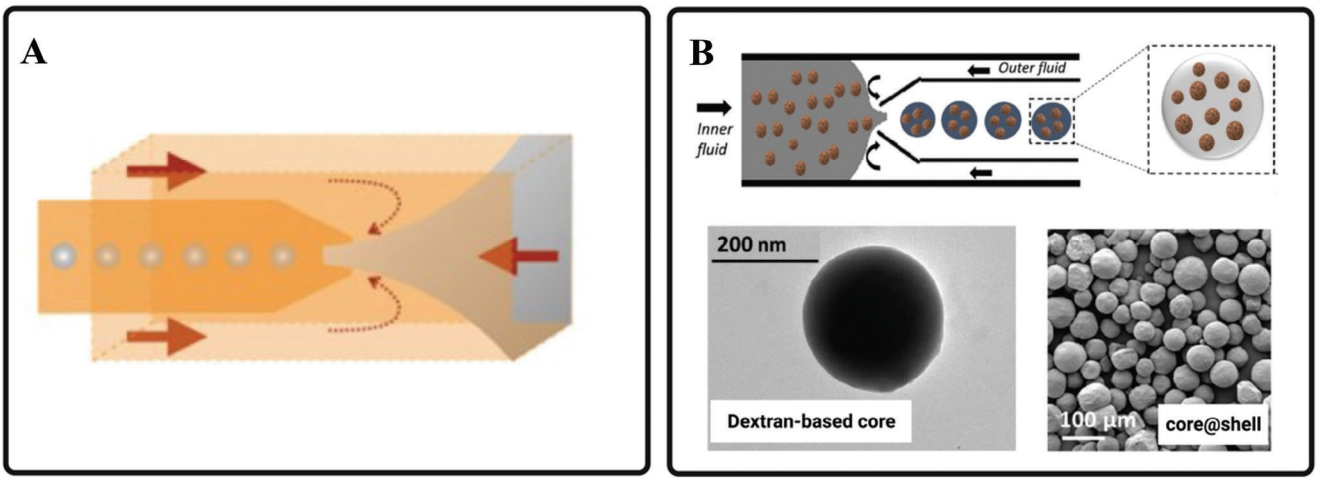

Figure 10. A) Glass capillary-based 3D axisymmetric flow focusing geometry; reproduced under the terms of the CC BY 4.0 license.[130] Copyright 2013, MDPI; B) ROS- and pH nano-micro composites; reproduced with permission.[133] Copyright 2024, John Wiley and Sons.

3.5. Co-Flow Mixing

In a co-flow geometry, all phases flow together in parallel streams, which can be in a 2D (achieved through soft lithography) or a cylinder-like (using glass capillaries) configuration.[134] Co-flow geometry it is frequently associated with flow focusing architecture, leading to a co-flow focused geometry. Like HHF, 3D geometry reduces the interaction between the particles and the walls, enhancing the control of the particle size and avoiding their deposition on the walls of the collecting channel (**Figure 11**A). In droplet-based MFs, the size of the resulting droplets is larger than the dimension of the dispersed microchannel (*wd*) when droplets are produced in dripping or widening jetting mode in most cases. However, there are exceptions, such as when the continuous phase flows at very high speeds, which can lead to a narrowing jet and even a tip-streaming regime.[135] The effectiveness of droplet production and the size of the droplets can both be controlled with this method by adjusting the continuous and dispersed phase flow rates.[136] Tahir et al. (2020) compared this method with BN in the production of LPNPs loaded with sorafenib (SFN).[101] While the BN method allowed the synthesis of adequate NPs, it was outperformed by the MF approach in SFN entrapment efficiency, control of particle size, and polydispersity index (PDI), further showcasing MFs as a better synthesis method in the field of nanomedicine. This methodology has also been mostly explored for the synthesis of polymeric CSNPs, as detailed in **Table 4**. For example, Liu et al. developed advanced CSNPs consisting of an encapsulated porous silicon NP surrounded by acetalated dextran shell for controlling the release of the loaded active ingredients (Figure 11B).[137] The one-step self-assembly approach employed in this study not only enhanced the surface smoothness and size distribution but also significantly improved the cytocompatibility of the particles.

This method has shown to be limited by the difficulty in reliably producing the microdevice, as well as by a low drug encapsulation efficiency.[141] This might explain the extensive range of obtained NP diameters.

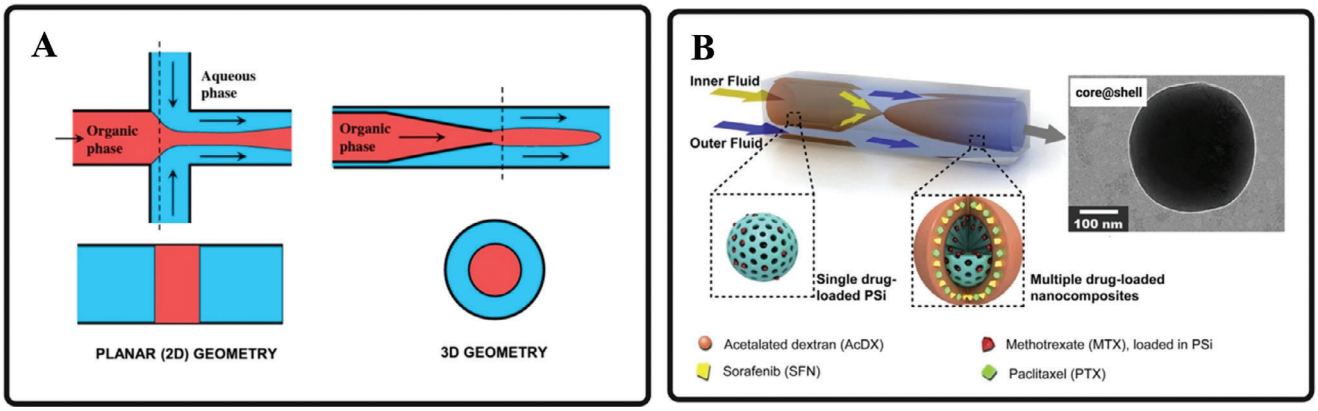

Figure 11. A) Longitudinal and cross-section cuts of 2D and 3D coflow devices; reproduced with permission.[138] Copyright 2024, Elsevier B.V; B) Nanoprecipitation-based synthesis of porous silicon (Psi) encapsulated Ac-DEX core/shell NPs in a coflow microchannel. Reproduced with permission.[137] Copyright 2024, Elsevier B.V.

Table 4. Co-flow setups in CSNP synthesis for drug delivery in cancer therapy.

Core@Shell	NP size/nm	Active agent	Outer channel diameter [mm]	Inner channel diameter [mm]	Ref.
PSi@Dextran	150 – 400	PTX, SFN, MTX	1	0.58	[137]
PLGA@Dextran	60 – 450	PTX and SFN	–	–	[139]
TAG@Dextran	95 – 266	–	1.12	0.58	[100]
PLGA/Lecithin@DSPE-PEG	190 – 300	SFN	–	–	[101]
PCL-b-PEG	< 80	SFN	1.10	0.58	[140]

DSPE: Distearoyl-α-cephalin; MTX: methotrexate; PCL: Polycaprolactone; PEG: polyethylene glycol; PLGA: poly-lactic-co-glycolic acid; PSi: porous silicon particle; PTX: paclitaxel; SFN: sorafenib; TAG: triacilglycerides.

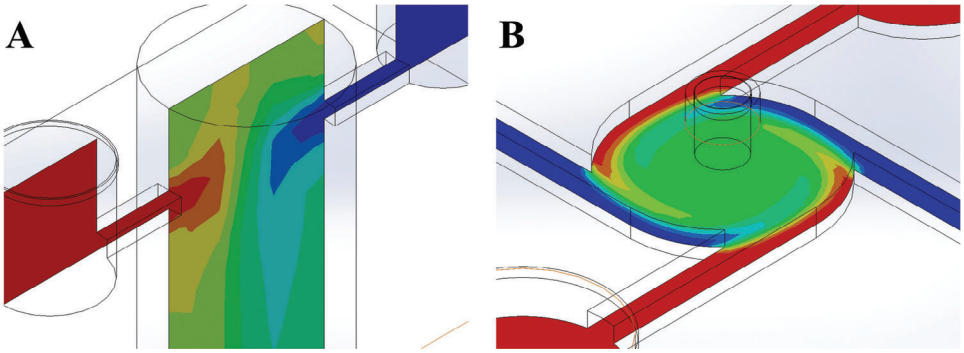

Figure 12. Schematics of A) CIJM; B) MIVM.

3.6. Alternative Strategies and Devices

In 2003, Johnson and Prud'Homme introduced the CIJM,[142] which has two opposing fluids rapidly pumped (with similar flow rates to prevent backflow) that collide into a mixing chamber to reduce the scale of segregation between the micro-volume liquid streams (**Figure 12**A).[143] In addition, the chamber size, geometry, different jet diameters, and outlet configurations determine the mixer performance.[144] Although this method has been used as a millifluidic system, MF variants have also been developed to produce NPs (**Table 5**). As an example, Lim et al. set a jet mixer capable of synthesizing PLGA-PEG NPs, lipidic micelles, iron oxide NPs, and polystyrene NPs, all of which around the 100 nm scale and encapsulating active agents like anticancer drugs and siRNA.[145] Indeed, this approach has demonstrated a higher versatility in terms of the fabrication of different types of NPs since using CIJM devices facilitates meeting the requirements to achieve a high mixing rate.[146] First, a high turbulent kinetic energy dissipation, which occurs at the collision point of the two streams, is achieved. Second, this high kinetic energy dissipation region expands into the mixing chamber. This kinetic energy takes longer to dissipate at greater inlet velocities (high *Re* flows), having an interesting effect on mixing because more energy is dissipated in the region where both fluids are present, thus facilitating the mixing of the fluid flow at small scale as Madadi-Kandjani et al. demonstrated in their simulations (**Figure 13**).[147] Specifically, a $Re = 310$ required almost three times less residence time than $Re = 62$ to reach a steady working condition. Besides, the $Re = 310$ showed that the two fluids were optimally mixed at a faster pace.

Since the CIJM requires streams with similar flow rates, the critical supersaturation concentration achievement is limited in this setup. Therefore, Prud'homme et al. introduced the MIVM setup, which allows for the operation with unequal flow

Table 5. MF jet mixing in CSNPs synthesis for drug delivery in cancer therapy.

Core@Shell	NP size [nm]	Active agent	Channel diameter [mm]	Reactor diameter [mm]	Flow rate [mL mi^{-1}n]	Ref.
PTX-silicate@PEG-b-PLGA	80 – 150	PTX	–	–	–	[148]
PLGA-PEG	30 – 200	Dtxl/Insulin	–	–	200 – 480	[145]
Lipid Vesicle	80 – 200	Fluorescent dye	–	–	31 – 313	
PLA-b-PLA	70	CUR	–	–	–	[149]
Florfenicol@PCL/PLGA	100 – 400	Florfenicol	1	4.8	80	[150]

CUR: curcumin; Dtxl: Docetaxel; PCL: polycaprolactone; PEG: polyethylene glycol; PLA: poly-lactic acid; PLGA: poly-lactic-co-glycolic acid; PTX: paclitaxel.

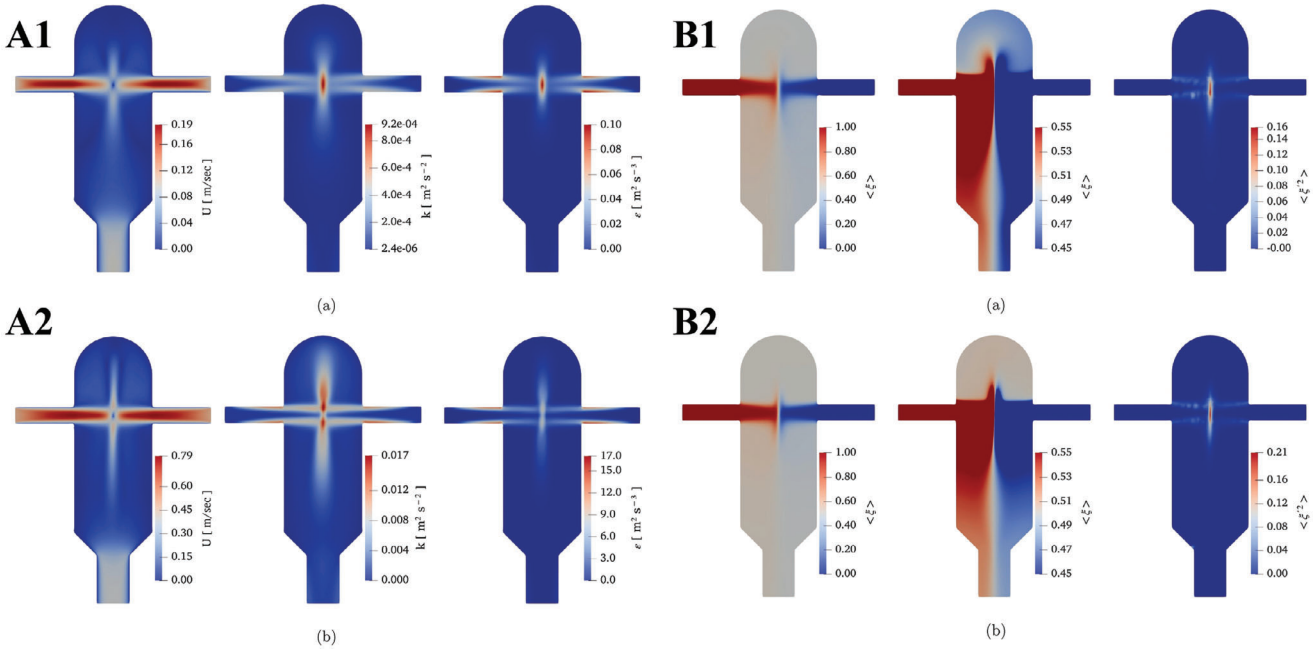

Figure 13. Simulation results from Madadi-Kandjani et al. Magnitude of the velocity, turbulent kinetic energy, and turbulence dissipation rate contour plots for Re = 62 at time 5 seconds (A1) and Re = 310 at time 1.75 seconds (A2). Mean mixture fraction (left and middle) and the mixture fraction variance (right) contour plots for Re = 62 at time 5 seconds (B1) and Re = 310 at time 1.75 seconds (B2). Reproduced under the terms of the CC BY 4.0 license.[147] Copyright 2013, Elsevier B.V.

ratios (Figure 12B).[151] This setup features a mixing chamber equipped with four inlets, and the liquid streams converge at an angle unlike in the CIJM, making it much more versatile.[143]

The MIVM's unique design enables a more rapid and efficient mixing within milliseconds, achieved through vortex forces. With its four inlet streams, micromixing can be independently controlled in the vortex chamber, offering greater flexibility in the nano-formulation process since each stream contributes independently to the mixing process in the mixing chamber.[152] On the one hand, the flow rate of solution and anti-solvent in the mixer chamber can be freely adjusted to achieve different supersaturation levels. Therefore, the nucleation and growth time can be manipulated on purpose. On the other hand, the high-efficiency and rapid mixing process of solvent and anti-solvent fluids ensures a short mixing time rather than nucleation and growth time of NPs.

Moreover, MIVM can be applied to various solvent ratios and materials.[144] This versatility can be harnessed to enhance the nanoprecipitation method, resulting in the production of drug-loaded NPs with consistent size and reproducibility.[153,154] Similar to other MF setups, the channels in the MIVM can be replaced by micromixing channels like the herringbone patterned design to improve the uniformity and size of the resulting particles significantly.[155] Recently, Zheng et al. demonstrated that introducing chaotic advection to a single-phase flow in tortuous channels at a sufficiently high *Re* within the laminar region enhances mixing.[154] This work, along with a few other examples of MIVM's application in the synthesis of CSNPs can be found in **Table 6**.

To overcome limitations related to monodispersity, mixing time, and particle size, researchers have explored inducing turbulent flow to promote rapid mixing.[19,96] One approach involves

Table 6. MIVM approaches in CSNP synthesis for drug delivery in cancer therapy.

Core@Shell	NP size [nm]	Active agent	Channel diameter [mm]	Reactor diameter [mm]	Flow rate 1 [mL $mi^{-1}n$]	Flow rate 2 [mL $mi^{-1}n$]	Ref.
β-carotene @PL/PEI/CH	< 100	*β*-carotene	–	–	13.3	120	[156]
β-carotene@ PEO-b-PS/ PEG-b-PCL	25 – 50	*β*-carotene	1.19	6.26	–	–	[153]
PEG-b-PCL	130 – 210	*β*-carotene	–	6	6	24 – 78	[51]
PC liposome	< 200	Lysozyme and erythromycin	1.13	5.92	4 – 20	–	[154]

CH: chitosan; PC: phosphatidylcoline; PCL: polycaprolactone; PEI: polyethyleneimine; PEG: polyethylene glycol; PEO: poly-(ethylene oxide); PL: polylysine; PS: polystyrene.

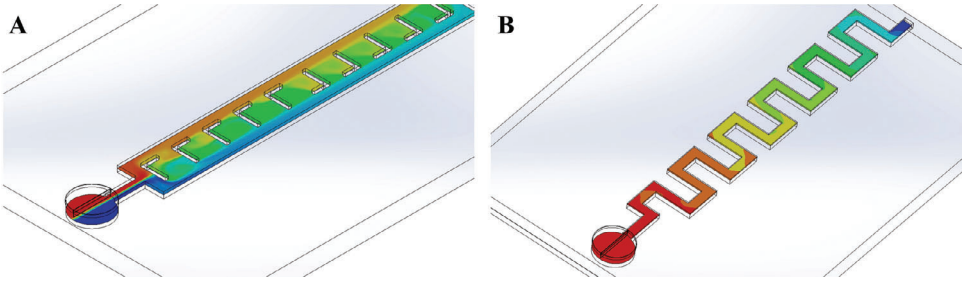

Figure 14. Scheme of chaotic advection micromixing channels: A) SHM; B) BM.

incorporating additional features into existing passive micromixing designs to generate turbulent flow regimes within laminar flow systems, such as micromixing channels (**Figure 14**).

The use of such devices can accelerate the mixing in the low *Re* regime by incorporating specific design elements, like baffles or grooves, which create a chaotic flow.[155] Alternatively, employing active micromixing techniques, such as acoustic micromixing, provides enhanced control and tunable properties through the introduction of an external energy source.[10] For instance, Valencia et al. demonstrated that the application of heat and/or sonication with rapid mixing enabled the formation of monodisperse particles that could be finely tuned in both size and charge due to their surface modification with lipids.[96] These advancements aim to enhance the efficiency and versatility of MFs in NPs synthesis, addressing the challenges associated with passive diffusive mixing and improving the overall production process.[10] However, considering the literature in this field, such techniques do not represent the norm. Micromixers based on chaotic flow are much more prominent, likely due to their reproducibility. Although any long channel capable of disturbing laminar flow can be used as a micromixer, this review considers the two main setups: the SHM and the BM.

The SHM induces micromixing through chaotic advection, in which the flow is disturbed using grooves. These herringbone structures are intricately designed on the microchannel floor, with pre-determined factors such as asymmetry, number, depth, and width of the grooves, all of which impact the mixing efficiency of the microchannel.[10] Chaotic advection reduces the mixing time especially at lower flow rates, resulting in less dilution and shorter processing times for NPs synthesis.[157]

Several studies have employed SHM to synthesize various CSNPs.[127,158] This setup may be particularly beneficial to produce LNPs, as its high mixing rate can cause an increase in lipid polarity, which leads to a supersaturation and a quick formation of LNPs.[126] This high efficiency in NPs synthesis achieved with SHM has led to its recognition as being supper-level to the simple HFF setup,[158] particularly when stacked with additional channels. An attempt that shows the advanced effectiveness of a multiple SHM-based MF device was exemplified by Shepherd et al.[159] In this work, a parallelized MF device (PMD), which includes a set of sequential SMH channels, was created. By increasing the area in which the phases interact with each other, the authors observed a significant increase in the throughput of over 100-fold when compared to a single channel SHM, HFF, and simple T-junctions, further presenting the up-scalability potential of MF devices that may pave the way to industrial MF production of nanomaterials for cancer medicine. However, the primary limitation of SMH channels, when compared to other micromixers, is the accumulation of precursor material in their grooves, which may lead to the clogging of the channels.[127] Also, the complex structure of this channel makes it more challenging to produce with the conventional methods.[61] Therefore, micromixers without grooves, such as baffle mixers, could be considered a viable alternative.

BM consists of serial turns that disturb the streams, agitating, stretching, and folding the flow of mass transfer.[160] In these micromixers, both the height and angles between baffles can significantly affect the mixing index of the fluids.[161] One of the most impactful attempts to utilize such a device was conducted by Kimura et al., who developed the invasive LNP production (iLiNP) device, a baffle micromixing channel capable of tuning the size of LNPs by intervals of 10 nm, down to a 20 nm NP diameter.[127] The efficacy of this setup was contrasted against standard BM and SHM devices. It was observed that, while the BM system could produce NPs as small as 20 nm with a flow rate of 500 µL mi^{-1}n and a Flow Ratio Rate of 9, the SHM could not achieve this. Additionally, the 2D structure of the BM allowed for more flexible production of LNPs compared to the SHM. As a result, the former was considered more useful for synthesizing small-sized and size-controlled nanocarriers. While still relatively uncommon in the literature related to CSNPs for cancer treatment, BMs belong to a broad category of advection-based systems. Many of these systems show an excellent ability to tune the size of NPs. Consequently, unless strict NP size standards are necessary, ease of production may be preferred. There is a large variety of unique baffle architectures. 2D setups, such as the asymmetrical split-and-recombine baffle micromixer,[162] may be easier to fabricate and integrate into a MF device. On the other hand, 3D setups, like the spiral BM,[163] provide greater flexibility in achieving optimal mixing but come with the trade-off of being more challenging to incorporate.

4. MF-Made CSNP Formulations in Cancer-Targeted Delivery

Research and development in cancer-targeted nanomedicine still see consistent growth, especially regarding novel techniques to optimize the size, multistep functionalities, reproducibility, and large-scale fabrication.[42] In an attempt to improve on the marketed nanomedicines, many methods are employed when producing CSNPs: nanoprecipitation, extrusion, micro-emulsion, solvent emulsification evaporation, among others.[164,165] While

Table 7. Examples of MF-fabricated CSNPs for cancer diagnostics and/or therapy in preclinical trials.

MF method	NP	Cancer	Active agent	In vitro	In vivo	Application	Ref
BM	LNP	Liver	SFN and siRNA	HepG-2	BCm	Chemotherapy	[167]
HFF	Liposome	Breast	Near-IR fluorescent dye	MCF-7	BCm	Tumor targeting	[20]
	LNP	Carcinoma	siRNA	KB/WT	–	Chemotherapy	[120]
	LPNP	Glioblastoma	IRI and Gd-DTPA	U87 MG	–	Theranostics	[122]
	P/LNPs-BM	Liver	VEGF siRNA	HepG-2	–	Chemotherapy	[168]
	CH-Magnetic NP	Ovaries	Cisplatin	A2780	–	Chemotherapy	[99]
	Liposome	Ovaries	Near-IR fluorescent dye	SKOV3	BCm	Tumor targeting	[20]
	PEI-b-PCL@Lipids	Prostate	siRNA	PC-3	BCm	Chemotherapy	[52]
CFM	FeTPt@CCM	Breast	FeTPt	4T1	BCm	Ferroptosis	[169]
	$Cu(DDC)_2$@BSA	Breast	$Cu(DDC)_2$	4T1	BCm	Chemotherapy	[170]
CFM/SHM	LPNP	Cervical	pDNA	CaSki	–	Chemotherapy	[126]
CFNP	LPNP	Colon	SFN	HT29-MTX	–	Chemotherapy	[101]
	LPNP	Breast	SFN	(MDA-MB-231	–	Chemotherapy	[101]
	LPNP	Prostate	SFN	PC3-MM2	–	Chemotherapy	[101]

BCm: Balb-C mice; BM: Baffle Mixing; BSA: Bovine Serum Albumin; CCM: Cancer cell membrane; CFM: Crossflow mixing; CFNP: Coflow-aided nanoprecipitation; CH: chitosan; DDC: Diethyldithiocarbamate; HFF: Hydrodynamic Flow Focusing; IRI: irinotecan; LNP: Lipid NP; LPNP: Lipid-polymer NP; MF: MF method; PCL: Polycaprolactone; pDNA: Plasmid DNA; SFN: Sorafenib; SHM: Staggered Herringbone Micromixing; VEGF: Vascular endothelial growth factor.

each approach has its own pros and cons, the inclusion of MFs may improve many of these technologies. For example, nanoprecipitation, a method that has historically been used by itself to produce NPs, is now commonly aided by MF setups to produce monodisperse CSNPs.[19,150,153,154]

Commonly produced using the HFF method,[20,52,122] chaotic advection-based micromixers such as the SHM channel,[10] and droplet-based MFs,[166] particles like LNPs can encapsulate a wide range of active agents, such as lipophilic molecules. **Table 7** summarizes recent CSNP formulations created by various MF techniques and validated through in vitro and in vivo preclinical trials.

The fabrication of NPs using MFs is a relatively recent topic and, consequently, biological studies are still in their early stages. As illustrated in Table 7, in vitro studies are currently more common in the literature than in vivo studies. Interestingly, all the showcased in vivo studies were performed on Balb-C mice.[20,52,167]

It is worth noting that all the showcased examples considered either chemotherapy.[52,99,101,126,167–169] or chemo-based theragnostic.[122] Following the use of PTX and DOX as the main staples in the field of cancer nanomedicine, SFN has risen as a promising alternative. It achieved the distinction of being the first FDA-approved drug for patients with advanced hepatocellular carcinoma, or HCC,[171] a cancer type known for its challenging tumor targetability due to the influence of the tumor stroma.[172] However, despite this agent's efficacy as a tyrosine kinase inhibitor, it lacks the bioavailability and compatibility to be delivered without a carrier.[173] Furthermore, its use can lead to the development of drug resistance within just 6 months.[171] To improve the efficacy of this agent in breast, colon, and prostate cancer, Tahir et al. developed core-shell LPNPs by nanoprecipitation, aided by the coflow MF technique.[101] This approach was contrasted against the BN method using the same formulation. Some of the results are showcased in **Figure 15**.

MF-produced NPs presented an encapsulation efficiency ranging from 87.4 to 97.0%, distinctly higher than the 83.8 to 90.0% observed in the particles made by BN (Figure 15A). This difference was attributed to the smaller relative size and PDI in MF-produced NPs, resulting from reduced mixing times caused by the limited space in MF channels. In addition, the BN-made NPs displayed a faster release, likely due to SFN adsorption on their surface. In contrast, the lower release seen in NPs fabricated with the MF device was linked to a higher degree of encapsulation and surface coating. As depicted in Figure 15B-C, this variance in morphology and encapsulation efficiency translated into enhanced cell growth inhibition. The delivery of naked SFN did not show an accentuated contrast to the treatment with BN-NPs. However, the MF-made NPs clearly outperformed their counterparts.

Another alternative to organic chemotherapeutical agents is cisplatin. This compound, which has been used to target cancer in the lungs, bladder, cervix, and ovaries, acts by undergoing hydrolysis upon entering cells, after which it becomes a strong electrophile capable of binding to purine residues in DNA. This process damages the DNA, triggering the activation of the p53 gene, which suppresses tumoral growth.[174] However, it is essential to note that this mechanism comes at the cost of high cytotoxicity. To counteract this toxicity issue, Siavashy et al. designed magnetic core/chitosan shell NPs via HFF to serve as carriers capable of delivering cisplatin, along with the complexing agent tripolyphosphate (TPP), without unwanted leakage.[99] This production method was compared to the standard batch flow method. In vitro cell viability studies conducted with A2780 cells (ovarian cancer cells) showed that the MF-made NPs (MSNs) caused lower viability when compared to batch flow-made ones. Additionally, the cellular uptake of Pt was more pronounced and sustained when delivered by MSNs, which also presented a lower degree of cisplatin release over time. Overall, MF-produced NPs consistently achieved superior biological performance than carriers prepared using conventional methods. However, platinum-based compounds have shown unwanted adverse effects, namely regarding toxicity.

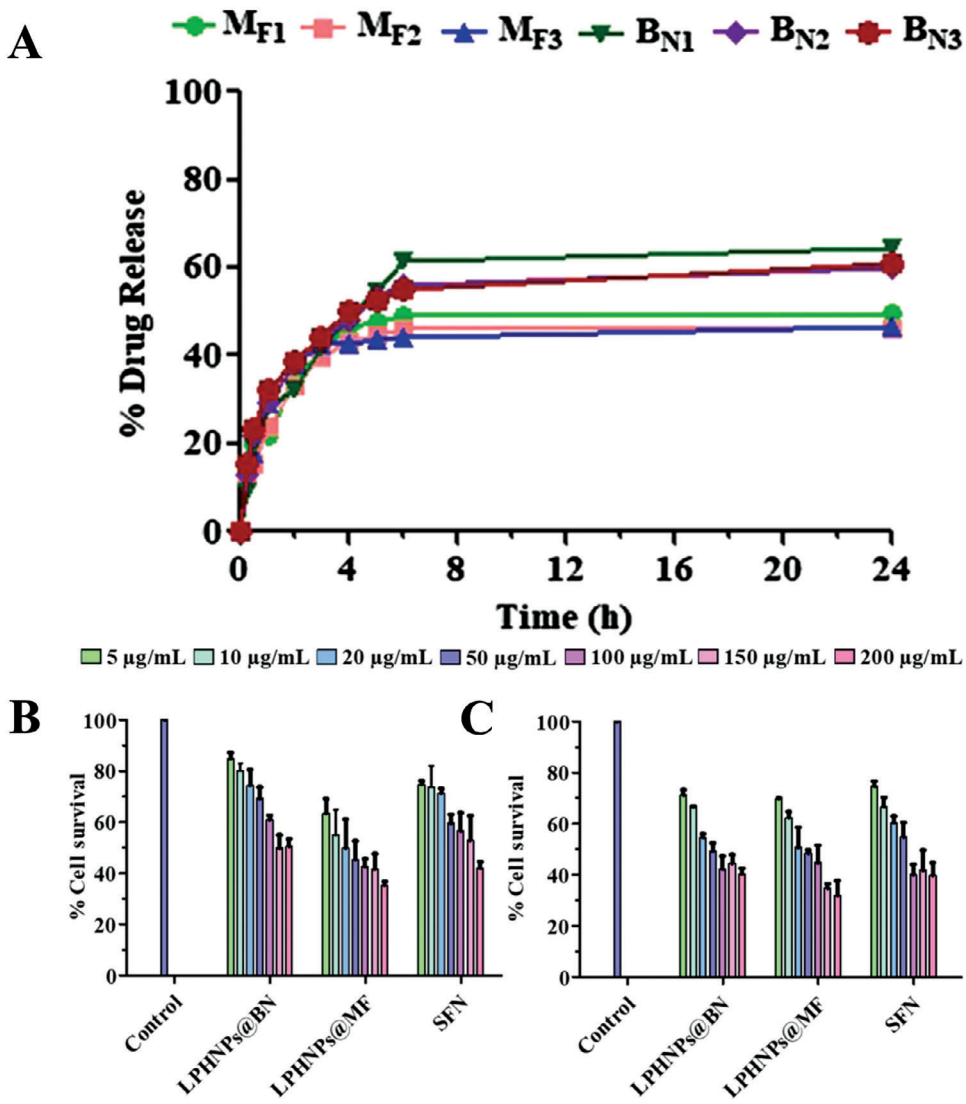

Figure 15. A) % of drug release seen in NPs prepared by BN and MFs; B) Degree of cell survival in the different therapeutical formulations in MDA-MB-231 cells and in C) PC3-MM2 cells. Reproduced with permission.[101] Copyright 2020, Elsevier B.V.

Metal-organic frameworks (MOF)-based delivery systems can be used as an alternative to such agents. These carriers have shown an excellent potential for drug delivery in cancer therapy, allowing for different therapeutic approaches, namely ferroptosis, a type of programmed cell death caused by iron-dependent oxidative stress.[175] Recently, Zhang et al. developed a MOF delivery system for tumor therapy using MFs (**Figure 16**).[169]

This multi-biomimetic MOF delivery system for combined ferroptosis therapy, chemotherapy, and photodynamic therapy (Figure 16A) was produced via MFs (Figure 16B). After delivery to the cytoplasm, the NPs can gather and enter the tumor, after which the platinum is reduced, releasing ferric ions that result in the generation of OH radicals for ferroptosis (Figure 16C). Figure 16D–G shows TEM images of FeT NPs, which display a homogenous morphology and distribution of Pt. In Figure 16H,I, fluorescence images of tumor-bearing mice and organs after injection of FeTPt and FeTPt@CCM NPs show a peak in distribution to the tumor, kidneys, and liver, with a much higher accumulation being seen in the CSNPs, in relation to the pure FeTPt group, an effect that the authors attributed to the camouflaging properties of CCM. Figure 16J shows a scheme of the phototherapeutic strategy used with this approach. After NP accumulation into the tumor, the surrounding area is irradiated with a 671 nm (red light) laser, which is in the "therapeutic window", the nanometer range in which light penetrates biological tissues most deeply.[176] The graph in Figure 16K shows the tumoral size as a function of time, for each of the therapeutic approaches. The FeTPt@CCM NPs showed the most effective anti-tumoral action, even without irradiation, when compared to the other strategies.

While compounds like cisplatin, PTX, and DOX have been staples of the field of nanomedicine, a new trend in cancer therapy that has increased in frequency is the delivery of siRNA. This shift is primarily due to the significant advantages offered by RNA-based therapies over the delivery of common chemo-based

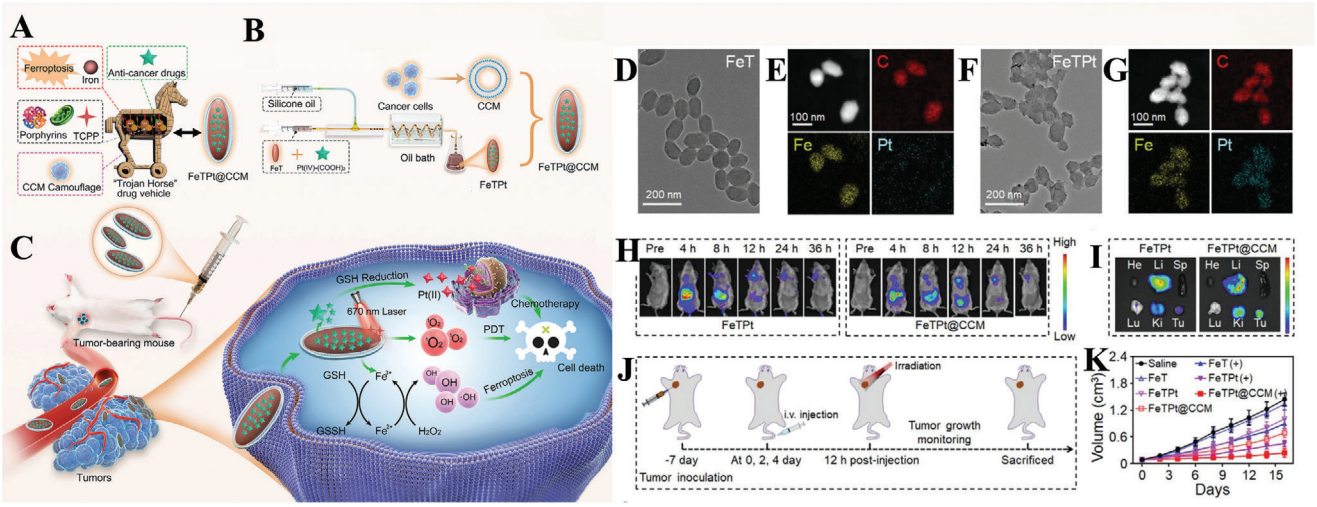

Figure 16. A) The concept of the multi-functional "Trojan Horse"-like drug vehicle; B) MF synthesis of FeTPt and subsequent coating with cell membrane (CCM) to form FeTPt@CCM; C) Efficient accumulation of FeTPt@CCM at the tumor site and its internalization into cancer cells through endocytosis upon intravenous injection.; D-G) Transmission electron microscopy (TEM) images and elemental mapping of (D,E) FeT and (F,G) FeTPt; H) In vivo fluorescence images of tumor-bearing mice (n = 3) post intravenous injection of FeTPt and FeTPt@CCM. I) Fluorescence images depicting major organs and tumors 12 hours after intravenous injection of FeTPt and FeTPt@CCM. J) Schematic representation of the therapeutic schedule. K) Tumor growth curves following different treatment approaches. Reproduced under the terms of the CC BY 4.0 license.[169] Copyright 2013, John Wiley and Sons.

agents. The delivery of siRNA has demonstrated remarkable efficacy even at reduced doses, resulting in limited side effects and reduced development of drug resistance.[160] However, it is essential to note that delivering naked siRNAs often results in ineffective therapies due to their limited intracellular intake, which is why they are commonly encapsulated in LNPs. Carriers like these are ideal for intracellular delivery not only because they are recognizable by the cells but also because the lipids interact with the polyanionic RNA, which results in a condensation of the particle to an ideal surface charge and size.[177] Since the launch of Patisiran, the first siRNA-based drug, subsequent research has consistently aimed at advancing the state of the art in this field (Table 7). Particularly, one of the foremost goals in this field is the development of reliable lipid-based delivery systems that can enable an adequate therapy, an aim which MF technology has significantly advanced.[178]

Wei et al. employed the HFF methods to engineer core@shell@shell NPs formed by lipid/PCL-PEI/siRNA for the delivery of siRNA.[52] They created a multi-inlet MF device in which aqueous siRNA was pumped through a middle inlet and encapsulated by a PEI-PCL polymeric micelle coming from lateral inlets in the form of PCL-PEI dissolved in DMSO. These initial particles were subsequently mixed with water from a second pair of lateral inlets, which were finally merged with a middle inlet pumping a lipophilic solution containing DOPE, DSPE-PEG, and cholesterol, encasing the particles in a lipidic vesicle. The NPs produced from this three-step emulsification method referred to as LPS were compared to those made through bulk mixing synthesis, designated as LMS, as depicted in **Figure 17A**. In this process, siRNA was pumped against the PEI-PCL solution coming from the sides, facilitating electrostatic interactions between PEI and siRNA, allowing the formation of PCL-PEI/siRNA complexes (represented in Figure 17D). Subsequent water pumping further along the process enables the assembly of the complexes into reverse micelles by inducing a solvent-switching effect. Finally, the lipidic solution resulting from the last step stabilized the reverse micelles, forming an outer layer that included PEG.

In this study, both in vitro and in vivo tests were performed, to ascertain the degree of tumor growth and map NP distribution in circulation. Notably, it was seen that the LPS NPs could distinctly outperform the LMS NPs in terms of relative tumor growth suppression (Figure 17B), with a difference of approximately 27%. This discrepancy was attributed to a superior encapsulation stability in the MF-made NPs, allowing them to retain siRNA for more extended periods and provide better protection during circulation. These findings were further supported by the results from excised *ex-vivo* tumors, as shown in Figure 17E. Concerning in vivo distribution (Figure 17C), LPS particles achieved a more intense and durable fluorescence in the overall tissues, except for the liver, after a specific period, suggesting a better accumulation and lower retention, which itself indicates improved biosafety. In contrast, the LMS particles triggered a more pronounced inflammatory response, attributed to a higher leakage of materials from the core, namely siRNA and PEI. Given the increased inhibition of tumoral growth, superior distribution, and stability in circulation observed with the LPS particles, the authors concluded that MFs hold promise as an approach for the delivery of siRNA in future clinical use.

Acknowledging the potential of siRNA and the historical use of SFN in cancer therapy, Younis et al. sought to combine the properties of these active agents in HCC therapy. To achieve this, they developed ultra-small LNPs (usLNPs) to co-deliver SFN and Midkine (MK)-siRNA.[167] The objective was to reverse the resistance to SFN and synergistically eradicate HCC in mice. These NPs were prepared using the aforementioned iLiNP device (a BM device), and their performance was compared to the NPs made using the film hydration method, referred to as

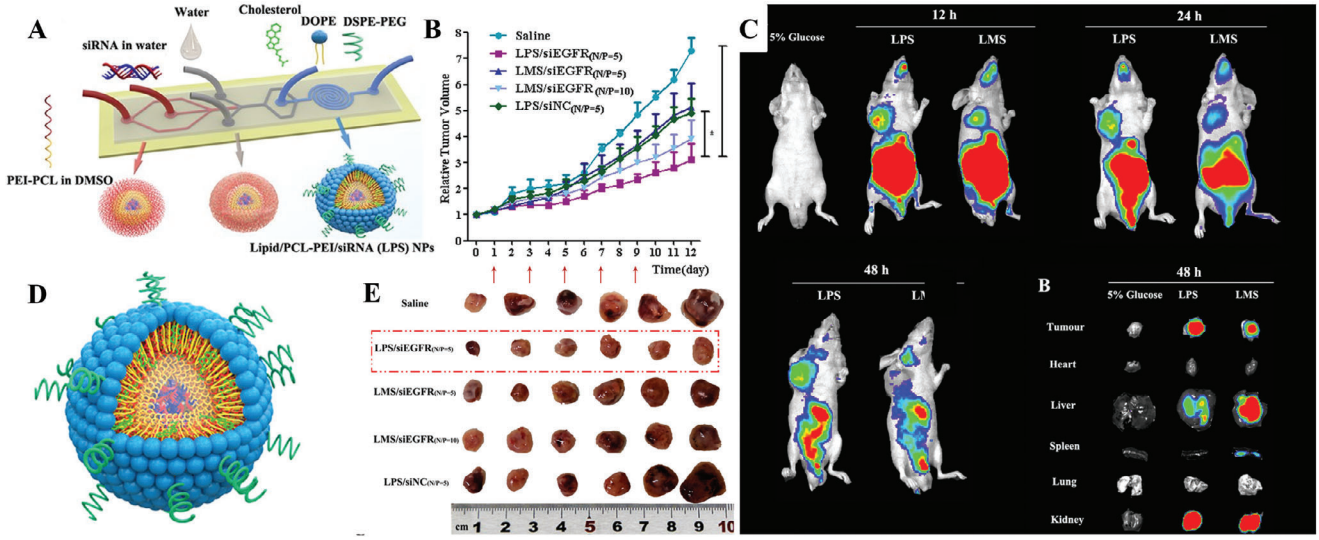

Figure 17. MF synthesis of LPNP-encapsulated siRNA: A) MF HFF device; B) Relative tumor volume as a function of time after treatment; C) In vivo cell distribution map; D) LPS concept; E) *Ex-vivo* tumors excised from nude mice after treatment. Adapted with permission.[52] Copyright 2024, American Chemical Society.

HEPES, named after the buffer that was used in the process. Despite the ultra-small size of the usLNPs, which enable them to effectively penetrate the stroma barrier, they also suffered issues from poor stability in circulation, as serum components that were quickly absorbed into the extremely high surface area of these NPs. The authors concluded that a size range of 70 – 100 nm was optimal for achieving maximum gene knock-down efficiency and tumor selectivity with the produced usLNPs. The in vivo results are showcased in **Figure 18**.

As seen in Figure 18A, therapy with SFN+MK-siRNA NPs resulted in a significant ≈85% inhibition of tumor growth, in stark contrast to the 40% and 18% inhibition caused by the SFN and siRNA monotherapies, respectively. This data is further illustrated in Figure 18B, which highlights the difference in tumor growth among the several treatment groups. Moreover, Figure 18C illustrates the survival rates of the various groups of HCC-bearing mice tested. The SFN+MK-siRNA NPs significantly extended the survival of these mice during the 60-day period of the study in comparison to the monotherapies. The enhanced efficacy observed in the MF-made NPs was attributed to their improved stability, which was achieved through an optimal size and size distribution that balanced stroma permeability with stability in circulation. Consequently, these particles exhibited reduced siRNA leakage, which translated into an increase in MK gene silencing within the tumor and a decreasing silencing in healthy tissues.

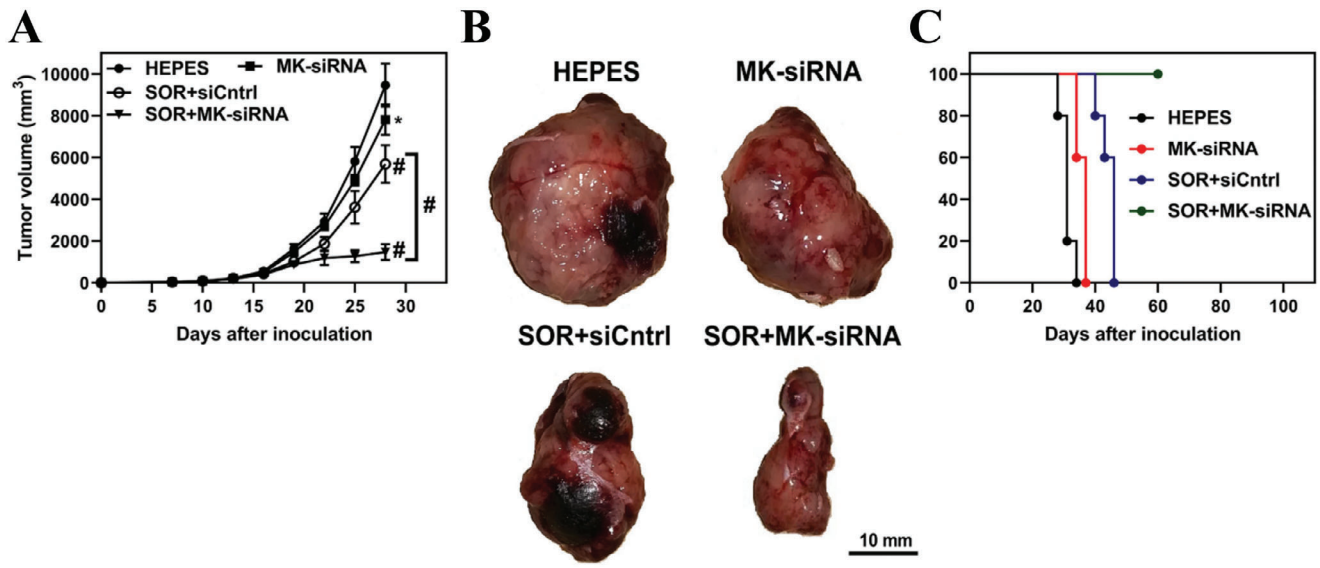

Figure 18. A) Tumor volume as a function of time after inoculation; B) *Ex-vivo* tumors excised from mice after treatment; C) Survival rates of mice after inoculation. Adapted with permission.[167] Copyright 2021, Elsevier B.V.

Table 7 also prominently highlights other HFF-made lipid-based nanocarriers.[20,99,122,168] In the context of LNPs and their hybrid counterparts, the preference for HFF over other MF methods can be attributed to the simplicity of processing with an HFF MF device. It often does not require a complex micromixing channel and can also be easily scalable. Some of the studies discussed have shown that a custom MF device allows the formulation of NPs with specific capabilities, especially when incorporating micromixers. For instance, in the work of Quagliarini et al., they employed a Y-junction + SHM channel setup to fabricate both PEGylated and unPEGylated DNA-loaded LNPs.[126] The authors reported a significant difference in the size of unPEGylated particles, particularly between LNPs produced at a flow rate of 2 mL $mi^{-1}n$ (LNP_2) and those at 8 mL $mi^{-1}n$ (LNP_8). This difference was not as pronounced in their PEGylated counterparts, likely due to the anti-aggregation effect of PEG, resulting in a lower degree of interactions between particles. This gap in particle size also translated into variations in biological properties. The transfection efficiency and cell viability were both notably higher in LNP_2, and this difference became even more pronounced with a higher concentration of pDNA in the inner core of the LNPs. Works like this underscore the clear advantage of using different MF methods in CSNP synthesis. When treating a cancer in which the EPR effect is weak, as is the case with HCC, one might opt for a device that allows the synthesis of ultra-small NPs, such as the iLiNP.[127,167] Conversely, in situations where an extremely small scale is not necessary, such as in many nanomedicinal lung cancer therapy approaches,[179] the emphasis may be on achieving long-term stability. In such cases, a multiple-step HFF device could be employed to produce core@shell@shell NPs, ensuring the attainment of maximum tumor selectivity.

Nowadays, in nanomedicine, MFs are applied not only in the synthesis of particles but also in several other ways. For example, in a recent study by Caputo et al., SFN-loaded PLGA particles were developed for HCC therapy.[173] These particles were designed to undergo UV-triggered release directly onto the tumor site using side-emitting optical fibers. While the fabrication was done through emulsion-solvent evaporation, a MF device was used to transport the particles to the target site, as depicted in the setup. The authors accomplished an impressive drug loading of 9%, a record value for SFN-loaded PLGA particles, along with a sustained release over 220 hours coupled with a high cellular uptake. Beyond this specific example, MFs as a technology are currently being applied in many ways to advance progress in nanomedicine. Gimondi et al. has recently published a review listing the diverse applications of MF devices not only as synthesis platforms but also for testing nanomedicinal formulations.[83] This work gathers examples of MF devices being employed as in vitro models to simulate in vivo conditions, whether by replicating blood vessels, as demonstrated in work by the same research group,[180] or by platforming 3D tumor models, such as tumors-on-a-chip.[181]

5. Discussion

Effectiveness in cancer therapy remains a key challenge in the field of medicine, as specific approaches can inadvertently harm healthy tissues. To tackle this issue, recent research has prominently focused on personalized therapies, nanotechnology, and targeted drug delivery. NPs, particularly CSNPs, exhibit promise in controlled drug release, minimizing side effects. CSNPs can be designed to safely carry a wide array of different active agents while also being optimized to target specific organs and tumors. Drug delivery for precise targeting is categorized into active and passive targeting, depending on the mechanism that leads the nanocarrier to the targeted site. Passive targeting appears to be the most exploited strategy due to its simplicity and lack of additional processing of particles, which can be expensive and time-consuming. Active targeting, in contrast, is usually reserved for the delivery of encapsulants that do not easily cross cell membranes.[27] The commonly adopted strategy of passive targeting, which relies on the EPR effect, may be hindered as the nanocarriers may get sequestered by the liver and spleen or eliminated by kidneys, to a degree that is proportional to the size of the carriers. Because of this, MF technology has gained popularity in the field of nanomedicine, as it serves as a reliable, reproducible, customizable, and easily controlled strategy to produce size-controlled particles in the micro and nanoscale. Although there are many different MF setups, a few have stood out for this purpose, particularly those based on continuous flow, which allows for a narrower size distribution of particles. HFF and co-flow mixing are the most applied setups, with and without advection-based micromixing channels. This is because they are the most reliable ways of producing size-controlled lipid-based particles, which are the most prominent carriers, due to the ideal tuneability and biological properties they display. Methods like MIVM and CJIM have fallen into disuse in NP synthesis, as they do not pose reliable alternatives to their microchannel-based counterparts. Other less conventional setups have been employed. Open microfluidic systems can be easier to use and have fewer clogging problems but lack the reliability in producing monodisperse particles in the nanoscale, and a sufficiently high throughput. 3D microchannel-based devices can allow for a narrower size distribution of particles but are more challenging to fabricate.[182]

Despite LNPs being the most common materials for the synthesis of drug delivery systems, they are closely followed by polymers, both synthetic (like PLGA and PCL) and derived from natural sources (e.g., dextran and CH). This is due to the high tuneability and simplicity of production, seeing as different polymeric mixtures can be designed to obtain desired properties. Encapsulants like PTX, CUR, SFN, and DOX have become standard in the field of oncology. However, recently, the therapeutic delivery of alternative agents like cisplatin, siRNA, and pDNA has grown in popularity, by allowing a more effective therapeutical action. This development is mostly a result of advancements in nanotechnology, which have enabled a more reliable fabrication of size and property-controlled carriers. In particular, the property control precision of MF devices has made viable the delivery of otherwise unstable agents. siRNA, which is almost completely ineffective when delivered nakedly, had been encapsulated in nanocarriers (mainly LNPs) without MF assistance, but their efficacy and viability was significantly hindered by low size control, monodispersity, scalability, and reproducibility.[183] The use of MF devices allows these otherwise unviable agents to now be stably stored and carried in controlled lipid vesicles. Particularly, it can be seen that the delivery of cisplatin benefits greatly from the added stability of MF-produced nanocarriers, seeing as metal-based therapies can

be quite toxic if not adequately targeted. And although a low upscalability of this process had been seen as a challenge in moving forward, devices like the PMD[159] or the iLiNP.[127] are paving the way to an industrial MF production of nanomaterials with new and optimal properties. The main drawback of resorting to this technology, as of now, is the low availability of MF devices resultant of the high cost and extremely specialized machinery that they require.

Additionally, despite the many uses for MFs in chemo-based nanomedicine, there is a noticeable gap in the field of targeted delivery for radiotherapy due to the inherent challenges it features. Tumors are frequently adjacent to radiation-sensitive tissues, which limits the potency of the applied therapy.[184] The field of MFs may be able to fill this gap by providing reliable and monodisperse nanocarriers capable of delivering radiosensitizers before irradiation, or in neutron capture therapy. As such, the implementation of MF systems in the production of carriers for targeted nanomedicine practices is significantly advancing the field of medicine to achieve more effective and safer strategies to challenge one of the most significant causes of death worldwide.

6. Conclusion

Although nanomedicine has demonstrated promising results in recent years, its efficacy largely hinges on the reproducibility of producing monodisperse stable NPs that can withstand leakage of the active agents before reaching the target site. MFs consistently present a better alternative to conventional methods of synthesizing nanocarriers, especially in the field of targeted nano-oncology, since it enables the fabrication of more precisely size and structure-tuned CSNP. The development of LNPs and LPNPs, in particular, appears to benefit the most from the use of MF devices, which can allow the formation of highly complex multiphasic structures with potential for multifunctional action. This advancement in complex design and tuneability is allowing the development of novel therapeutic strategies capable of safely storing agents like siRNA and cisplatin, which, despite having presented a significant anti-cancer potential, have seen their viability limited by carrying instability. Additionally, the fact that different sets of microchannels can be treated as individual modules and combined with other systems defines this technology as extremely versatile, enabling the precise fabrication of highly customizable and complex multi-phasic delivery systems. HFF systems, though commonly employed individually and for the fabrication of LNPs, are capable not only of delivering new compounds, but also of being applied in multifunctional therapeutic strategies.

However, for the complete leap to MFs to be made, some challenges have yet to be overcome:

Technical challenges: the need for multidisciplinary teams limits the extensiveness of research and development in smaller groups and institutes will less resources.

Biological challenges: good efficacy in preclinical studies does not necessarily translate into good efficacy in humans due to the unpredictability of the nanomedicine field. NP efficacy relies on the accumulation and entry of NPs into the tumor microenvironment and the controlled drug release only at the target site, both of which are difficult to control in a complex in vivo system.

Technological challenges: continuous-flow MFs suffer from issues like the viscous drag in the microchannels that causes nonuniform velocities, which results in a less monodisperse distribution of NPs. Additionally, there is an unavoidable accumulation of material inside the walls of MF devices, which not only puts these on a timer but also limits the possibility of scaling up the synthesis process to be able to work on an industrial scale. The fabrication of MF devices is expensive and requires specified machinery. Also, since many works may require a custom-built device, the development and sale of standardized devices – which could allow for higher accessibility – is not always viable.

Economic challenges: for a new medicinal formulation to enter the market, the efficacy and safety must be proven statistically, which means an extensive time and money-heavy study must be made.

Acknowledgements

The financial support of TEMA is also acknowledged by the projects UIDB/00481/ 2020 and UIDP/00481/2020 from FCT and CENTRO-01-0145-FEDER-022083—Centro Portugal Regional Operational Program (Centro 2020), under the PORTUGAL 2020 Partnership Agreement, through the European Regional Development Fund. This work was also developed within the scope of the project CICECO-Aveiro Institute of Materials, UIDB/50011/2020, UIDP/50011/2020 and LA/P/0006/2020, financed by national funds through the FCT/MCTES (PIDDAC). The research contract of R.J.B. Pinto was funded by national funds (OE), through FCT in the scope of the framework contract foreseen in the numbers 4, 5, and 6 of the article 23, of the Decree-Law 57/2016, of August 29, changed by Law 57/2017, of July 19. The authors also acknowledge the financial support of project CARBONCT (2022.03596.PTDC; https://doi.org/10.54499/2022.03596.PTDC). J.F.G. thanks FCT for the PhD grant UI/BD/151259/2021. H. A. Santos acknowledges financial support from the Academy of Finland (Decision no. 331151) and the UMCG Research Funds.

Conflict of Interest

The authors declare no conflict of interest.

Keywords

multiphasic nanoparticles, nanomedicine, theragnostic microfluidics, tumor targeting

Received: March 13, 2024
Revised: May 9, 2024
Published online:

[1] Global Cancer Observatory, "Cancer Today," **2023**. (accessed: July 2023).
[2] American Cancer Society **2007**. (accessed: July 2023).
[3] L. Racca, V. Cauda, *Remotely Activated Nanoparticles for Anticancer Therapy*, Springer, Singapore **2021**.
[4] P. M. Giri, A. Banerjee, B. Layek, *Cancers* **2023**, *15*, 2256.
[5] K. Powell, *Nature* **2009**.
[6] D. Peer, J. M. Karp, S. Hong, O. C. Farokhzad, R. Margalit, R. Langer, *Nat. Nanotechnol.* **2007**, *2*, 751.
[7] E. Bottaro, A. Mosayyebi, D. Carugo, C. Nastruzzi, *Micromachines (Basel)* **2017**, *8*, 1.

[8] G. Gonçalves, S. Sandoval, M. Llenas, B. Ballesteros, T. Da Ros, S. Bortolussi, L. Cansolino, C. Ferrari, I. Postuma, N. Protti, M. Melle-Franco, S. Altieri, G. Tobías-Rossell, *Carbon* **2023**, *208*, 148.
[9] M. J. Mitchell, M. M. Billingsley, R. M. Haley, M. E. Wechsler, N. A. Peppas, R. Langer, *Nat. Rev. Drug Discov.* **2021**, *20*, 101.
[10] Y. Liu, G. Yang, Y. Hui, S. Ranaweera, C. X. Zhao, *Small* **2022**, *18*, 1.
[11] I. U. Khan, C. A. Serra, N. Anton, T. Vandamme, *J. Controlled Release* **2013**, *172*, 1065.
[12] R. Ghosh Chaudhuri, S. Paria, *Chem. Rev.* **2012**, *112*, 2373.
[13] S. Yazdian Kashani, A. Afzalian, F. Shirinichi, M. Keshavarz Moraveji, *RSC Adv.* **2021**, *11*, 229.
[14] A. S. Yadav, D. T. Tran, A. J. T. Teo, Y. Dai, F. M. Galogahi, C. H. Ooi, N. T. Nguyen, *Micromachines (Basel)* **2023**, *14*, 497.
[15] M. H. M. Leung, T. Harada, S. Dai, T. W. Kee, *Langmuir* **2015**, *31*, 11419.
[16] A. Nagayasu, K. Uchiyama, H. Kiwada, *Adv. Drug Deliv. Rev.* **1999**, *40*, 75.
[17] B. Ouyang, W. Poon, Y.-N. Zhang, Z. P. Lin, B. R. Kingston, A. J. Tavares, Y. Zhang, J. Chen, M. S. Valic, A. M. Syed, P. MacMillan, J. Couture-Senécal, G. Zheng, W. C. W. Chan, *Nat. Mater.* **2020**, *19*, 1362.
[18] N. Hoshyar, S. Gray, H. Han, G. Bao, *Nanomedicine* **2016**, *11*, 673.
[19] L. Capretto, W. Cheng, D. Carugo, O. L. Katsamenis, M. Hill, X. Zhang, *Nanotechnology* **2012**, *23*, 375602.
[20] R. Ran, H. Wang, Y. Liu, Y. Hui, Q. Sun, A. Seth, D. Wibowo, D. Chen, C.-X. Zhao, **2018**, 1.
[21] L. Shi, J. Zhang, M. Zhao, S. Tang, X. Cheng, W. Zhang, W. Li, X. Liu, H. Peng, Q. Wang, *Nanoscale* **2021**, *13*, 10748.
[22] S. Wilhelm, A. J. Tavares, Q. Dai, S. Ohta, J. Audet, H. F. Dvorak, W. C. W. Chan, *Nat. Rev. Mater.* **2016**, *1*, 16014.
[23] C. He, Y. Hu, L. Yin, C. Tang, C. Yin, *Biomaterials* **2010**, *31*, 3657.
[24] S. Hirn, M. Semmler-Behnke, C. Schleh, A. Wenk, J. Lipka, M. Schäffler, S. Takenaka, W. Möller, G. Schmid, U. Simon, W. G. Kreyling, *Eur. J. Pharm. Biopharm.* **2011**, *77*, 407.
[25] A. Saikia, R. Newar, S. Das, A. Singh, D. J. Deuri, A. Baruah, *Chem. Eng. Res. Des.* **2023**, *193*, 516.
[26] R. K. Thapa, J. O. Kim, *J. Pharm. Investig.* **2023**, *53*, 19.
[27] M. F. Attia, N. Anton, J. Wallyn, Z. Omran, T. F. Vandamme, *J. Pharm. Pharmacol.* **2019**, *71*, 1185.
[28] T. Lammers, F. Kiessling, W. E. Hennink, G. Storm, *J. Controlled Release* **2012**, *161*, 175.
[29] B. Begines, T. Ortiz, M. Pérez-Aranda, G. Martínez, M. Merinero, F. Argüelles-Arias, A. Alcudia, *Nanomaterials* **2020**, *10*, 1403.
[30] L. Bregoli, J. Lysaght, J. Reynolds, A. Prina-Mello, Nanomedicine Applied to Translational Oncology: A Future Perspective on Cancer Treatment Short Title: Nanomedicine Applied to Translational Oncology **2015**.
[31] Y. N. Zhang, W. Poon, A. J. Tavares, I. D. McGilvray, W. C. W. Chan, *J. Controlled Release* **2016**, *240*, 332.
[32] N. Rolley, M. Bonnin, G. Lefebvre, S. Verron, S. Bargiel, L. Robert, J. Riou, C. Simonsson, T. Bizien, J.-C. Gimel, J.-P. Benoit, G. Brotons, B. Calvignac, *Nanoscale* **2021**, *13*, 11899.
[33] L. Zhang, Q. Chen, Y. Ma, J. Sun, *ACS Appl. Bio Mater.* **2020**, *3*, 107.
[34] C. Khanna, M. Rosenberg, D. M. Vail, *J. Vet. Intern. Med.* **2015**, *29*, 1006.
[35] T. Hamaguchi, Y. Matsumura, M. Suzuki, K. Shimizu, R. Goda, I. Nakamura, I. Nakatomi, M. Yokoyama, K. Kataoka, T. Kakizoe, *Br. J. Cancer* **2005**, *92*, 1240.
[36] Y. Tsukioka, Y. Matsumura, T. Hamaguchi, H. Koike, F. Moriyasu, T. Kakizoe, *Jpn. J. Cancer Res.* **2002**, *93*, 1145.
[37] Z. Cheng, A. Al Zaki, J. Z. Hui, V. R. Muzykantov, A. Tsourkas, *Science* **2012**, *338*, 903.
[38] X. Kang, H. H. Xiao, H. Q. Song, X. Bin Jing, L. S. Yan, R. G. Qi, *Cancer Biol. Med.* **2015**, *12*, 362.
[39] L. C. Gomes-Da-Silva, N. A. Fonseca, V. Moura, M. C. Pedroso De Lima, S. Simões, J. N. Moreira, *Acc. Chem. Res.* **2012**, *45*, 1163.
[40] T. Nakamura, H. Harashima, *Adv. Drug. Deliv. Rev.* **2020**, *167*, 78.
[41] Y. Barenholzt, S. Amselem, L. D., *FEBS Lett.* **1979**, *99*, 210.
[42] M. Maeki, N. Kimura, Y. Sato, H. Harashima, M. Tokeshi, *Adv. Drug Deliv. Rev.* **2018**, *128*, 84.
[43] S. M. Rafiyath, M. Rasul, B. Lee, G. Wei, G. Lamba, D. Liu, *Exp. Hematol. Oncol.* **2012**, *1*, 10.
[44] H. He, D. Yuan, Y. Wu, Y. Cao, *Pharmaceutics* **2019**, *11*.
[45] A. J. Guillot, M. Martínez-Navarrete, T. M. Garrigues, A. Melero, *J. Controlled Release* **2023**, *355*, 624.
[46] R. M. Haley, R. Gottardi, R. Langer, M. J. Mitchell, *Drug Deliv. Transl. Res.* **2020**, *10*, 661.
[47] R. Karnik, F. Gu, P. Basto, C. Cannizzaro, L. Dean, W. Kyei-Manu, R. Langer, O. C. Farokhzad, *Nano Lett.* **2008**, *8*, 2906.
[48] S. Rezvantalab, M. Keshavarz Moraveji, *RSC Adv.* **2019**, *9*, 2055.
[49] B. L. Sanchez-Gaytan, F. Fay, M. E. Lobatto, J. Tang, M. Ouimet, Y. Kim, S. E. M. van der Staay, S. M. van Rijs, B. Priem, L. Zhang, E. A. Fisher, K. J. Moore, R. Langer, Z. A. Fayad, W. J. M. Mulder, *Bioconjugate Chem.* **2015**, *26*, 443.
[50] A. Bains, Y. Cao, S. Kly, J. E. Wulff, M. G. Moffitt, *Mol. Pharmaceutics* **2017**, *14*, 2595.
[51] Z. Fu, L. Li, M. Wang, X. Guo, *Colloid Polym. Sci.* **2018**, *296*, 935.
[52] W. Wei, J. Sun, X. Y. Guo, X. Chen, R. Wang, C. Qiu, H. T. Zhang, W. H. Pang, J. C. Wang, Q. Zhang, *ACS Appl. Mater. Interfaces* **2020**, *12*, 14839.
[53] Y. Chai, Y. Wang, B. Li, W. Qi, R. Su, Z. He, *Langmuir* **2021**, *37*, 7219.
[54] D. Belletti, G. Riva, M. Luppi, G. Tosi, F. Forni, M. A. Vandelli, B. Ruozi, F. Pederzoli, *Eur. J. Pharm. Sci.* **2017**, *107*, 230.
[55] A. Fabozzi, F. Della Sala, M. Di Gennaro, A. Borzacchiello, *New J. Chem.* **2022**, *46*, 19763.
[56] W. T. Lim, E. H. Tan, C. K. Toh, S. W. Hee, S. S. Leong, P. C. S. Ang, N. S. Wong, B. Chowbay, *Ann. Oncol.* **2010**, *21*, 382.
[57] M. E. Werner, N. D. Cummings, M. Sethi, E. C. Wang, R. Sukumar, D. T. Moore, A. Z. Wang, *Int. J. Radiat. Oncol.* **2013**, *86*, 463.
[58] R. Ramos, J. Bernard, F. Ganachaud, A. Miserez, *Small Science* **2022**, *2*, 2100095.
[59] H. Xu, H. Ma, P. Yang, X. Zhang, X. Wu, W. Yin, H. Wang, D. Xu, *Colloids Surf., B* **2015**, *136*, 729.
[60] D. Chouhan, T. Lohe, P. K. Samudrala, B. B. Mandal, **2018**, *1801092*, 1.
[61] B. G. Carvalho, B. T. Ceccato, M. Michelon, S. W. Han, L. G. de la Torre, *Pharmaceutics* **2022**, *14*, 141.
[62] S. Hua, S. Y. Wu, *Front Pharmacol* **2013**, *4*.
[63] L. Sercombe, T. Veerati, F. Moheimani, S. Y. Wu, A. K. Sood, S. Hua, *Front Pharmacol* **2015**, *6*.
[64] Y. Barenholz, *J. Controlled Release* **2012**, *160*, 117.
[65] A. C. Anselmo, S. Mitragotri, *Bioeng. Transl. Med.* **2019**, *4*, 3.
[66] R. Kashapov, A. Ibragimova, R. Pavlov, D. Gabdrakhmanov, N. Kashapova, E. Burilova, L. Zakharova, O. Sinyashin, *Int. J. Mol. Sci.* **2021**, *22*.
[67] J. Gehl, M. Boesgaard, T. Paaske, B. Vittrup Jensen, P. Dombernowsky, *Ann. Oncol.* **1996**, *7*, 687.
[68] M. Rasool, A. Malik, S. Waqar, M. Arooj, S. Zahid, M. Asif, S. Shaheen, A. Hussain, H. Ullah, S. H. Gan, *Bioengineered* **2022**, *13*, 759.
[69] National Cancer Institute, Current Nanotechnology Treatments, **2023**. (accessed: September 2023).
[70] F. Rodríguez, P. Caruana, N. De la Fuente, P. Español, M. Gámez, J. Balart, E. Llurba, R. Rovira, R. Ruiz, C. Martín-Lorente, et al., *Biomolecules* **2022**, 12.
[71] F. Mahmud, K. F. Tamrin, *Asia-Pac. J. Chem. Eng.* **2020**, *15*, e2407.
[72] K. Abstiens, A. M. Goepferich, *J. Drug Deliv. Sci. Technol.* **2019**, *49*, 433.

[73] D. Liu, H. Zhang, F. Fontana, J. T. Hirvonen, H. A. Santos, *Adv. Drug Deliv. Rev.* **2018**, *128*, 54.
[74] T. Chen, Y. Peng, M. Qiu, C. Yi, Z. Xu, *Nanoscale* **2023**, *15*, 3594.
[75] T. M. Ho, A. Razzaghi, A. Ramachandran, K. S. Mikkonen, *Adv. Colloid Interface Sci.* **2022**, *299*, 102541.
[76] R. Djerafi, Y. Masmoudi, C. Crampon, A. Meniai, E. Badens, *J. Supercrit. Fluids* **2015**, *105*, 92.
[77] W. S. Saad, R. K. Prud'homme, *Nano Today* **2016**, *11*, 212.
[78] S. M. D'Addio, R. K. Prud'homme, *Adv. Drug Deliv. Rev.* **2011**, *63*, 417.
[79] C. J. Martínez Rivas, M. Tarhini, W. Badri, K. Miladi, H. Greige-Gerges, Q. A. Nazari, S. A. Galindo Rodríguez, R. Á. Román, H. Fessi, A. Elaissari, *Int. J. Pharm.* **2017**, *532*, 66.
[80] K. Y. Hernández-Giottonini, R. J. Rodríguez-Córdova, C. A. Gutiérrez-Valenzuela, O. Peñuñuri-Miranda, P. Zavala-Rivera, P. Guerrero-Germán, A. Lucero-Acuña, *RSC Adv.* **2020**, *10*, 4218.
[81] G. T. Vladisavljević, R. Al Nuumani, S. A. Nabavi, *Micromachines (Basel)* **2017**, *8*.
[82] Y. Amini, V. Ghazanfari, M. Heydari, M. M. Shadman, A. G. Khamseh, M. H. Khani, A. Hassanvand, *Sci. Rep.* **2023**, *13*, 9483.
[83] S. Gimondi, H. Ferreira, R. L. Reis, N. M. Neves, *ACS Nano* **2023**, *17*, 14205.
[84] J. Saliba, A. Daou, S. Damiati, J. Saliba, M. El-Sabban, R. Mhanna, *Genes (Basel)* **2018**, *9*.
[85] J. Atencia, D. J. Beebe, *Nature* **2005**, *437*, 648.
[86] R. P. Chhabra, V. Shankar, Institution of Chemical Engineers (Great Britain), in *Coulson and Richardson's Chemical Engineering (Seventh Edition)*, Butterworth-Heinemann, Kidlington **2018**, pp. 529–546.
[87] D. J. Beebe, G. A. Mensing, G. M. Walker, *Annu. Rev. Biomed. Eng.* **2002**, *4*, 261.
[88] D. Hernández-Cid, V. H. Pérez-González, R. C. Gallo-Villanueva, J. González-Valdez, M. A. Mata-Gómez, *Mater. Today: Proc.* **2022**, *48*, 30.
[89] J. K. Nunes, S. S. H. Tsai, J. Wan, H. A. Stone, *J. Phys. D: Appl. Phys.* **2013**, *46*, 114002.
[90] S.-K. Moon, I. W. Cheong, S.-W. Choi, *Colloids Surf., A* **2014**, *454*, 84.
[91] N. M. Kovalchuk, M. Sagisaka, K. Steponavicius, D. Vigolo, M. J. H. Simmons, *Microfluid. Nanofluid.* **2019**, *23*, 103.
[92] A. Venkateshwarlu, R. P. Bharti, *J. Taiwan Inst. Chem. Eng.* **2021**, *129*, 64.
[93] C. Shen, F. Liu, L. Wu, C. Yu, W. Yu, *Micromachines (Basel)* **2020**, *11*.
[94] É. Lepercq-Bost, M.-L. Giorgi, A. Isambert, C. Arnaud, *J. Membr. Sci.* **2008**, *314*, 76.
[95] F. Mardani, S. Falahatian, M. Taghipoor, *Results Eng.* **2023**, *18*, 101125.
[96] P. M. Valencia, P. A. Basto, L. Zhang, M. Rhee, R. Langer, O. C. Farokhzad, R. Karnik, *ACS Nano* **2010**, *4*, 1671.
[97] Y. Kim, F. Fay, D. P. Cormode, B. L. Sanchez-Gaytan, J. Tang, E. J. Hennessy, M. Ma, K. Moore, O. C. Farokhzad, E. A. Fisher, W. J. M. Mulder, R. Langer, Z. A. Fayad, *ACS Nano* **2013**, *7*, 9975.
[98] Y. Shen, S. A. Yuk, S. Kwon, H. Tamam, Y. Yeo, B. Han, *J. Controlled Release* **2023**, *357*, 484.
[99] S. Siavashy, M. Soltani, F. Ghorbani-Bidkorbeh, N. Fallah, G. Farnam, S. A. Mortazavi, F. H. Shirazi, M. H. H. Tehrani, M. H. Hamedi, *Carbohydr. Polym.* **2021**, *265*.
[100] J. Rosenfeld, F. Ganachaud, D. Lee, *Langmuir* **2023**, *39*, 5477.
[101] N. Tahir, A. Madni, W. Li, A. Correia, M. Muzamil, M. Abdur, H. A. Santos, *Int. J. Pharm.* **2020**, *581*, 119275.
[102] J. Zhou, A. V. Ellis, N. H. Voelcker, *ELECTROPHORESIS* **2010**, *31*, 2.
[103] C. F. Rodríguez, V. Andrade-Pérez, M. C. Vargas, A. Mantilla-Orozco, J. F. Osma, L. H. Reyes, J. C. Cruz, *Front. Bioeng. Biotechnol.* **2023**, *11*.
[104] M. de Almeida Monteiro Melo Ferraz, J. B. Nagashima, B. Venzac, S. Le Gac, N. Songsasen, *Sci. Rep.* **2020**, *10*, 994.
[105] D. Liu, S. Cito, Y. Zhang, C.-F. Wang, T. M. Sikanen, H. A. Santos, *Adv. Mater.* **2015**, *27*, 2298.
[106] M. Rhee, P. M. Valencia, M. I. Rodriguez, R. Langer, O. C. Farokhzad, R. Karnik, *Adv. Mater.* **2011**, *23*, H79.
[107] S. Kuddannaya, Y. J. Chuah, M. H. A. Lee, N. V. Menon, Y. Kang, Y. Zhang, *ACS Appl. Mater. Interfaces* **2013**, *5*, 9777.
[108] S. Hu, X. Ren, M. Bachman, C. E. Sims, G. P. Li, N. Allbritton, *Anal. Chem.* **2002**, *74*, 4117.
[109] N. Leister, G. T. Vladisavljević, H. P. Karbstein, *J. Colloid Interface Sci.* **2022**, *611*, 451.
[110] B. Herranz-Blanco, E. Ginestar, H. Zhang, J. Hirvonen, H. A. Santos, *Int. J. Pharm.* **2017**, *516*, 100.
[111] P.-C. Chen, M.-H. Wu, Y.-N. Wang, *Sensors Mater.* **2014**, *26*, 45.
[112] B. G. de Carvalho, T. B. Taketa, B. B. M. Garcia, S. W. Han, L. G. de la Torre, *Materials Science and Engineering C* **2021**, *118*.
[113] Y. Zeng, J. W. Khor, T. L. van Neel, W. chen Tu, J. Berthier, S. Thongpang, E. Berthier, A. B. Theberge, *Nat. Rev. Chem.* **2023**, *7*, 439.
[114] M. Gonidec, J. Puigmartí-Luis, *Crystals (Basel)* **2019**, *9*.
[115] J. Sun, L. Zhang, J. Wang, Q. Feng, D. Liu, Q. Yin, D. Xu, Y. Wei, B. Ding, X. Shi, X. Jiang, *Adv. Mater.* **2015**, *27*, 1402.
[116] L. Zhang, Q. Feng, J. Wang, J. Sun, X. Shi, X. Jiang, *Angew. Chem., Int. Ed.* **2015**, *54*, 3952.
[117] J. Sun, Y. Xianyu, M. Li, W. Liu, L. Zhang, D. Liu, C. Liu, G. Hu, X. Jiang, *Nanoscale* **2013**, *5*, 5262.
[118] Z. Huang, N. A. Mayr, W. T. C. Yuh, S. S. Lo, J. F. Montebello, J. C. Grecula, L. Lu, K. Li, H. Zhang, N. Gupta, J. Z. Wang, *Cancer Res.* **2010**, *70*, 463.
[119] A. Jahn, W. N. Vreeland, M. Gaitan, L. E. Locascio, *J. Am. Chem. Soc.* **2004**, *126*, 2674.
[120] R. Krzysztoń, B. Salem, D. J. Lee, G. Schwake, E. Wagner, J. O. Rädler, *Nanoscale* **2017**, *9*, 7442.
[121] A. Fabozzi, D. Sala, *New J. Chem.* **2022**, *46*, 19763.
[122] F. Roffo, A. M. Ponsiglione, P. A. Netti, **2022**.
[123] R. Seemann, M. Brinkmann, T. Pfohl, S. Herminghaus, *Rep. Prog. Phys.* **2012**, *75*, 016601.
[124] K. Loizou, V. L. Wong, B. Hewakandamby, *Inventions* **2018**, *3*.
[125] L. Sheng, L. Ma, Y. Chen, J. Deng, G. Luo, *Chem. Eng. J.* **2022**, *427*, 132067.
[126] E. Quagliarini, S. Renzi, L. Digiacomo, F. Giulimondi, B. Sartori, H. Amenitsch, V. Tassinari, L. Masuelli, R. Bei, L. Cui, et al., *Pharmaceutics* **2021**, *13*.
[127] N. Kimura, M. Maeki, Y. Sato, Y. Note, A. Ishida, H. Tani, H. Harashima, M. Tokeshi, *ACS Omega* **2018**, *3*, 5044.
[128] E. Lallana, R. Donno, D. Magrì, K. Barker, Z. Nazir, K. Treacher, M. J. Lawrence, M. Ashford, N. Tirelli, *Int. J. Pharm.* **2018**, *548*, 530.
[129] N. Kimura, M. Maeki, Y. Sato, Y. Note, A. Ishida, H. Tani, H. Harashima, M. Tokeshi, **2018**.
[130] J. M. Zhang, Q. Ji, H. Duan, *Micromachines (Basel)* **2019**, *10*.
[131] S. Takeuchi, P. Garstecki, D. B. Weibel, G. M. Whitesides, *Adv. Mater.* **2005**, *17*, 1067.
[132] D. Liu, H. Zhang, F. Fontana, J. T. Hirvonen, H. A. Santos, *Lab Chip* **2017**, *17*, 1856.
[133] S. Bertoni, Z. Liu, A. Correia, J. P. Martins, A. Rahikkala, F. Fontana, M. Kemell, D. Liu, B. Albertini, N. Passerini, W. Li, H. A. Santos, *Adv. Funct. Mater.* **2018**, *28*, 1806175.
[134] P. Zhu, L. Wang, *Lab Chip* **2017**, *17*, 34.
[135] A. S. Utada, A. Fernandez-Nieves, H. A. Stone, D. A. Weitz, *Phys. Rev. Lett.* **2007**, *99*, 094502.
[136] J. Liana, X. Luob, X. Huanga, Y. Wanga, Z. Xua, X. Ruanc, *Colloids Surf., A* **2019**, *568*, 381.
[137] D. Liu, H. Zhang, E. Mäkilä, J. Fan, B. Herranz-Blanco, C.-F. Wang, R. Rosa, A. J. Ribeiro, J. Salonen, J. Hirvonen, H. A. Santos, *Biomaterials* **2015**, *39*, 249.

[138] R. Othman, G. T. Vladisavljević, H. C. Hemaka Bandulasena, Z. K. Nagy, *Chem. Eng. J.* **2015**, *280*, 316.
[139] D. Liu, H. Zhang, S. Cito, J. Fan, E. Mäkilä, J. Salonen, J. Hirvonen, T. M. Sikanen, D. A. Weitz, H. A. Santos, *Nano Lett.* **2017**, *17*, 606.
[140] V. Känkänen, M. Fernandes, Z. Liu, J. Seitsonen, S. P. Hirvonen, J. Ruokolainen, J. F. Pinto, J. Hirvonen, V. Balasubramanian, H. A. Santos, *J. Colloid Interface Sci.* **2023**, *633*, 383.
[141] A. Fabozzi, F. Della Sala, M. di Gennaro, M. Barretta, G. Longobardo, N. Solimando, M. Pagliuca, A. Borzacchiello, *Lab Chip* **2023**, *23*, 1389.
[142] B. K. Johnson, R. K. Prud'homme, *AIChE J.* **2003**, *49*, 2264.
[143] J. Han, Z. Zhu, H. Qian, A. R. Wohl, C. J. Beaman, T. R. Hoye, C. W. Macosko, *J. Pharm. Sci.* **2012**, *101*, 4018.
[144] J. Tao, S. F. Chow, Y. Zheng, *Acta Pharm. Sin. B* **2019**, *9*, 4.
[145] J. M. Lim, A. Swami, L. M. Gilson, S. Chopra, S. Choi, J. Wu, R. Langer, R. Karnik, O. C. Farokhzad, *ACS Nano* **2014**, *8*, 6056.
[146] Y. Hao, J. H. Seo, Y. Hu, H. Q. Mao, R. Mittal, *AIP Adv.* **2020**, *10*.
[147] E. Madadi-Kandjani, A. Passalacqua, R. O. Fox, *Chem. Eng. Sci.* **2023**, *273*, 118634.
[148] J. Han, A. R. Michel, H. S. Lee, S. Kalscheuer, A. Wohl, T. R. Hoye, A. V. McCormick, J. Panyam, C. W. Macosko, *Mol. Pharmaceutics* **2015**, *12*, 4329.
[149] S. F. Chow, K. Y. Wan, K. K. Cheng, K. W. Wong, C. C. Sun, L. Baum, A. H. L. Chow, *Eur. J. Pharm. Biopharm.* **2015**, *94*, 436.
[150] L. N. Turino, B. Stella, F. Dosio, J. A. Luna, A. A. Barresi, *Drug Dev. Ind. Pharm.* **2018**, *44*, 934.
[151] Y. Liu, C. Cheng, Y. Liu, R. K. Prud'homme, R. O. Fox, *Chem. Eng. Sci.* **2008**, *63*, 2829.
[152] S. I. Hamdallah, R. Zoqlam, P. Erfle, M. Blyth, A. M. Alkilany, A. Dietzel, S. Qi, *Int. J. Pharm.* **2020**, *584*, 119408.
[153] H. Shen, S. Hong, R. K. Prud'Homme, Y. Liu, *J. Nanopart. Res.* **2011**, *13*, 4109.
[154] H. Zheng, H. Tao, J. Wan, K. Y. Lee, Z. Zheng, S. S. Y. Leung, *Pharmaceutics* **2022**, *14*, 1223.
[155] A. Bokare, A. Takami, J. H. Kim, A. Dong, A. Chen, R. Valerio, S. Gunn, F. Erogbogbo, *ACS Omega* **2019**, *4*, 4650.
[156] Z. Zhu, K. Margulis-Goshen, S. Magdassi, Y. Talmon, C. W. Macosko, *J. Pharm. Sci.* **2010**, *99*, 4295.
[157] T. P. Forbes, J. G. Kralj, *Lab Chip* **2012**, *12*, 2634.
[158] C. C. L. Cheung, W. T. Al-Jamal, *Int. J. Pharm.* **2019**, *566*, 687.
[159] S. J. Shepherd, C. C. Warzecha, S. Yadavali, R. El-Mayta, M. G. Alameh, L. Wang, D. Weissman, J. M. Wilson, D. Issadore, M. J. Mitchell, *Nano Lett.* **2021**, *21*, 5671.
[160] S. H. El Moukhtari, E. Garbayo, A. Amundarain, S. Pascual-Gil, A. Carrasco-León, F. Prosper, X. Agirre, M. J. Blanco-Prieto, *J. Controlled Release* **2023**, *361*, 130.
[161] M. Rasouli, A. Abouei Mehrizib, M. Goharimaneshc, A. Lashkaripourd, S. R. Bazaz, *Chem. Eng. Process.* **2018**, *132*, 175.
[162] W. Raza, K. Y. Kim, *Micromachines (Basel)* **2019**, *10*.
[163] S. Zhao, Y. Nie, W. Zhang, R. Hu, L. Sheng, W. He, N. Zhu, Y. Li, D. Ji, K. Guo, *Chin. J. Chem. Eng.* **2023**, *56*, 255.
[164] R. Paliwal, R. J. Babu, S. Palakurthi, *AAPS PharmSciTech* **2014**, *15*, 1527.
[165] U. Dristant, K. Mukherjee, S. Saha, D. Maity, *Technol. Cancer Res. Treat.* **2023**, *22*, 153303382311520.
[166] J. Ahn, J. Ko, S. Lee, J. Yu, Y. T. Kim, N. L. Jeon, *Adv. Drug Deliv. Rev.* **2018**, *128*, 29.
[167] M. A. Younis, I. A. Khalil, Y. H. A. Elewa, Y. Kon, H. Harashima, *J. Controlled Release* **2021**, *331*, 335.
[168] X. Huang, R. J. Lee, Y. Qi, Y. Li, J. Lu, Q. Meng, **2017**, *8*, 96826.
[169] Q. Zhang, G. Kuang, H. Wang, Y. Zhao, J. Wei, L. Shang, *Adv. Sci.* **2023**.
[170] Y. Chang, J. Jiang, W. Chen, W. Yang, L. Chen, P. Chen, J. Shen, S. Qian, T. Zhou, L. Wu, et al., *Appl. Mater. Today* **2020**, *18*.
[171] L. Guo, C. Hu, M. Yao, G. Han, *Front Pharmacol* **2023**, *14*.
[172] K. C. Valkenburg, A. E. De Groot, K. J. Pienta, *Nat. Rev. Clin. Oncol.* **2018**, *15*, 366.
[173] T. M. Caputo, A. M. Cusano, S. Principe, P. Cicatiello, G. Celetti, A. Aliberti, A. Micco, M. Ruvo, M. Tagliamonte, C. Ragone, M. Minopoli, M. V. Carriero, L. Buonaguro, A. Cusano, *Int. J. Nanomed.* **2023**, *18*, 4121.
[174] I. W. Achkar, N. Abdulrahman, H. Al-Sulaiti, J. M. Joseph, S. Uddin, F. Mraiche, *J Transl Med* **2018**, *16*.
[175] C. Zhang, X. Liu, S. Jin, Y. Chen, R. Guo, *Mol. Cancer* **2022**, *21*, 47.
[176] W. Sun, R. Thiramanas, L. D. Slep, X. Zeng, V. Mailänder, S. Wu, *Chem. Eur. J.* **2017**, *23*, 10832.
[177] T. C. Roberts, R. Langer, M. J. A. Wood, *Nat. Rev. Drug Discov.* **2020**, *19*, 673.
[178] N. Bargahi, S. Ghasemali, S. Jahandar-Lashaki, A. Nazari, *Biol. Proced. Online* **2022**, *24*, 5.
[179] J. Park, Y. Choi, H. Chang, W. Um, J. H. Ryu, I. C. Kwon, *Theranostics* **2019**, *9*, 8073.
[180] S. Gimondi, H. Ferreira, R. L. Reis, N. M. Neves, *ACS Appl. Nano Mater.* **2023**, *6*, 7364.
[181] J. F. Gil, C. S. Moura, V. Silverio, G. Gonçalves, H. A. Santos, *Adv. Mater.* **2023**.
[182] R. Su, F. Wang, M. C. McAlpine, *Lab Chip* **2023**, *23*, 1279.
[183] C. Lopes, J. Cristóvão, V. Silvério, P. R. Lino, P. Fonte, *Expert Opin. Drug Deliv.* **2022**, *19*, 1381.
[184] S. L. Liauw, P. P. Connell, R. R. Weichselbaum, *Sci. Transl. Med.* **2013**, *5*, 173sr2.

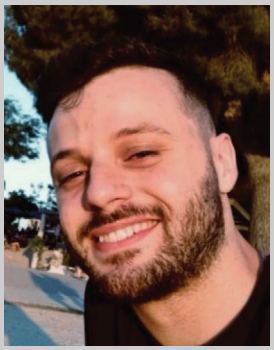

Duarte Almeida obtained his master's degree in "Biomedical Materials and Devices" from the Department of Materials and Ceramics Engineering, University of Aveiro. Currently, he is a PhD student in "Nanosciences and Nanotechnology" at the Centre for Mechanical Technology and Automation (TEMA-UA), Department of Mechanical Engineering, University of Aveiro, under the supervision of Dr. Gil Gonçalves. His research interests include microfluidics, carbon nanostructures, and nanoparticles as targeted delivery systems.

Ricardo J.B. Pinto graduated in Chemistry from the University of Porto in 2004 and received his MSc (2008) and PhD (2012) in Chemistry from the University of Aveiro. Currently, he is a Researcher at CICECO – Aveiro Institute of Materials, where his research is dedicated to the development of new green approaches for synthesizing metallic and polymeric nanoparticles and their application in the preparation of functional biocomposite materials.

Hélder A. Santos (D.Sc. Tech., Chem. Eng.) is a Full Professor at the Department of Biomaterials and Biomedical Technology and Head of the same Department at the University Medical Center Groningen, University of Groningen. His research interests include the development of nanoparticles, microparticles, nanomedicines, and biomaterials for biomedical and tissue engineering applications, particularly cancer and heart diseases. His lab makes the unique bridge between medical engineering and tissue engineering by combining unique techniques to develop novel therapeutic formulations for translation into the clinic.

Gil Gonçalves graduated in chemistry and received his Ph.D. in mechanical engineering at the University of Aveiro. In 2016, he started working at the Institute of Material Science of Barcelona (ICMAB-CSIC) on neutron capture therapy. He was a short-term visitor at the Laboratory of Applied Nuclear Energy–University of Pavia and at the Department of Chemical and Pharmaceutical Sciences, University of Trieste. Presently, he leads a dynamic research group at the Center for Mechanical Technology and Automation – University of Aveiro, delving into cutting-edge endeavors involving innovative carbon-based hybrid materials for cancer therapy and bioimaging, pioneering advancements in nanocomposite microfluidic fabrication, and the development of groundbreaking tumor-on-chip technology.